81.3 [(+)-**12**, 14.2%]. (+)-**13**: HPLC under the same conditions: t_R (min) = 21.8 [(–)-**13**, 7.5%], 23.9 [(+)-**13**, 92.5%].

To a mixture of alcohol (±)-**15** (10 mg, 0.037 mmol) in vinyl acetate (1 mL) was added *Candida rugosa* lipase (Meito OF, 10 mg) and the mixture was stirred for 16 h at room temperature. In the similar workup and separation as describe above, the corresponding (–)-acetate (5.1 mg, 41.8%) and (+)-**15** (4.4 mg, 44.0%) were obtained. (+)-**15**: HPLC analysis [column, Daicel Chiralcel OD-H, 0.46 cm × 25 cm; hexane-isopropyl alcohol (30:1); flow late 0.5 mL min^{-1}; detected at 210 nm]: t_R (min) = 32.7 [(+)-**15**, 88.9%], 37.1 [(–)-**15**, 11.1%]. The stereochemical assignment on the preferential enantiomer for **15** is based on the retention times on HPLC analysis. In the case of **12**, (+)-**12** showed shorter retention time than that of (–)-**12** in the use of Chiralcel OD-H, while (+)-**12** showed longer retention time than that of (–)-**12** on Chiralcel AY-3. Unfortunately, no good separation was observed between the enantiomers of **15** on Chiralcel AY-3. In the case of **15**, the conversion (44.7%) was determined by the comparison of peak area in ^{1}H NMR spectrum of crude reaction mixture: δ 6.75 (s, 1H, H-2 for **15**), 6.71 (s, 1H, H-2 for the acetate).

4.7. Ethyl (3R,4S,5R)-5-hydroxy-3,4-isopropylidenedioxycyclohex-1-enecarboxylate (17).

To a solution of (+)-**12** (1.4 g, 5.8 mmol) in CH_2Cl_2 (30 mL) were added pyridine (2.1 mL, 17.3 mmol), Tf_2O (3.1 mL, 11.5 mmol) and DMAP (170 mg, 1.20 mmol), and the mixture was stirred for 30 min at 0 °C. The reaction was quenched with saturated $NaHCO_3$ aq. solution and organic materials were extracted with EtOAc. The combined extract was washed with brine, dried over Na_2SO_4 and concentrated *in vacuo* to afford **16** as a colorless solid; yield: 2.2 g. This was employed for the next step without further purification.

To a solution of **16** (2.2 g, 5.87 mmol) in DMF (25 mL) was added KNO_2 (1.0 g, 11.8 mmol), and the mixture was stirred for 8 h at room temperature. The reaction was quenched with saturated 0.1 M phosphate buffer solution (pH 7.0) and organic materials were extracted with EtOAc. The combined extract was washed with brine, dried over Na_2SO_4 and concentrated *in vacuo*. The residue was purified by silica gel column chromatography (20 g). Elution with hexane-EtOAc (2:1) afforded (–)-**17** as a colorless oil (1.1 g, 75% over two steps). ^{1}H NMR ($CDCl_3$) δ 6.92 (s, 1H), 4.73 (m, 1H), 4.20 (q, J = 7.0 Hz, 2H), 4.06 (dd, J = 7.1, 6.9 Hz, 1H), 3.87 (ddd, J = 12.9, 8.6, 4.7 Hz, 1H), 2.79 (dd, J = 17.4, 4.7 Hz, 1H), 2.21 (dd, J = 17.4, 8.6 Hz, 1H), 1.43 (s, 3H), 1.38 (s, 3H), 1.27 (t, J = 7.0 Hz, 3H); $[\alpha]_D^{26}$ –33.0 (*c* 0.50, EtOAc) [lit.[10] $[\alpha]_D^{25}$ –31.0 (*c* 3.0, EtOAc)]. Its IR and NMR spectra were identical with those reported previously.[10]

4.8. Ethyl shikimate (1).

To a solution of the above-mentioned (–)-**17** (1.1 g, 4.3 mmol) in EtOH (20 mL) was added Dowex 50W-X8 acidic ion-exchange resin (2.0 g) and the mixture was stirred for 48 h at room temperature. The resin was filtered off, and the filtrate was concentrated *in vacuo*. The residue was purified by silica gel column chromatography (20 g). Elution with hexane-EtOAc (1:3) afforded (–)-**1** as a colorless solid (820 mg, 78%). ^{1}H NMR ($CDCl_3$) δ 6.88 (s, 1H), 4.46 (m, 1H), 4.20 (q, J = 7.2 Hz, 2H), 3.96 (dd, J = 8.8, 4.0 Hz, 1H), 3.61 (dd, J = 9.0, 4.0 Hz, 1H), 2.94 (dd, J = 17.4, 6.0 Hz, 1H), 2.20 (dd, J = 17.4, 8.8 Hz, 1H), 1.67 (bs, 2H), 1.27 (t, J = 7.2 Hz, 3H); $[\alpha]_D^{23}$ –97.6 (*c* 1.00, MeOH). Its ^{1}H NMR spectra was in good accordance with that of ethyl shikimate.[13]

4.9. Ethyl (3S,4S,5R)-5-acetoxy-3,4-dihydroxycyclohex-1-enecarboxylate (18).

To a solution of acetate (–)-**13** (6.7 g, 23 mmol) in CH_2Cl_2 (200 mL) was added $FeCl_3 \cdot 6H_2O$ (18 g, 69 mmol) and the mixture was stirred for 6 h at room temperature. The reaction was quenched with saturated $NaHCO_3$ aq. solution and organic materials were extracted with EtOAc three times. The combined extract was washed with brine, dried over Na_2SO_4, and concentrated *in vacuo*. The residue was purified by silica gel column chromatography (100 g). Elution with hexane-EtOAc (1:1) afforded **18** as a colorless solid (5.0 g, 87%). IR (neat) 3432, 2983, 1724, 1641, 1382, 1261, 1240, 1153, 1105 cm^{-1}; ^{1}H NMR ($CDCl_3$) δ 6.77 (s, 1H), 5.03 (dt, J = 5.9, 2.3 Hz, 1H), 4.39 (s, 1H), 4.19 (q, J = 7.1 Hz, 2H), 4.08 (d, J = 2.3 Hz, 1H), 2.64 (dd, J = 7.4, 5.9 Hz, 1H), 2.54 (dd, J = 7.4, 5.9 Hz, 1H), 2.09 (s, 3H), 1.28 (t, J = 7.1 Hz, 3H); ^{13}C NMR ($CDCl_3$) δ 171.5, 167.0, 138.4, 130.0, 72.0, 69.7, 68.7, 62.2, 27.0, 22.2, 15.2; $[\alpha]_D^{27}$ +26.2 (*c* 0.50, MeOH); mp 79.5-80.1 °C; Anal. Calcd for $C_{11}H_{16}O_6$: C, 54.09; H, 6.60; Found: C, 53.88; H, 6.56.

4.10. Ethyl shikimate (1) from 18.

To a solution of **18** (140 mg, 0.57 mmol) in THF (6 mL) was added Et_3N (320 μL, 2.28 mmol) and $SOCl_2$ (123 μL, 1.71 mmol) and the mixture was stirred for 30 min at 0 °C. The reaction was quenched with saturated $NaHCO_3$ aq. solution and organic materials were extracted with EtOAc. The combined extract was washed with brine, dried over Na_2SO_4 and concentrated *in vacuo* and afford **19** as a dark-colored oil (151 mg). This was employed for the next step without further purification.

To a solution of the above-mentioned **19** (151 mg, 0.52 mmol) in DMF (5 mL) was added CsOAc (200 mg, 1.04 mmol) and the mixture was stirred for 12 h at 40 °C. The reaction was quenched with saturated NH_4Cl aq. solution and organic materials were extracted with EtOAc. The combined extract was washed with brine, dried over Na_2SO_4 and concentrated *in vacuo* and afforded **20** as a yellow oil (89 mg). This was employed for the next step without further purification. ^{1}H NMR ($CDCl_3$) δ 6.70 (d, J = 2.5 Hz, 1H), 5.55 (dd, J = 5.9, 2.5 Hz, 1H), 5.28 (dd, J = 6.9, 4.5 Hz, 1H), 4.19 (q, J = 7.2 Hz, 2H), 3.94 (d, J = 5.9 Hz, 1H), 2.67 (dd, J = 16.2, 6.9 Hz, 1H), 2.66 (dd, J = 16.2, 4.5 Hz, 1H), 2.09 (s, 3H), 2.07 (s, 3H), 1.27 (t, J = 7.2 Hz, 3H).

To a solution of **20** (89 mg, 0.31 mmol) in CH_2Cl_2 (3 mL) were added pyridine (38 μL, 0.47 mmol), Tf_2O (76 μL, 0.47 mmol), and DMAP (3.6 mg, 0.03 mmol) and the mixture was stirred for 30 min at 0 °C. The reaction was quenched with saturated $NaHCO_3$ aq. solution and organic materials were extracted with EtOAc. The combined extract was washed with brine, dried over Na_2SO_4 and concentrated *in vacuo* to afford **21** as a yellow oil (130 mg). This was employed for the next step without further purification.

To a solution of the above-mentioned **21** (130 mg, 0.31 mmol) in DMF (3 mL) was added KNO_2 (53 mg, 0.62 mmol) and the mixture was stirred for 3 h at room temperature. The reaction was quenched with 0.1 M phosphate buffer solution (pH 7.0) and organic materials were extracted with EtOAc. The combined extract was washed with brine, dried over Na_2SO_4 and concentrated *in vacuo* to afford **22** as a colorless solid (40 mg). ^{1}H NMR ($CDCl_3$) δ 6.59 (s, 1H), 5.58 (d, J = 8.6 Hz, 1H), 5.07 (dd, J = 9.4, 8.3 Hz, 1H), 4.20 (q, J = 7.2 Hz, 2H), 3.95 (m, 1H), 2.96 (dd, J = 17.6, 8.3 Hz, 1H), 2.37 (dd, J = 17.6, 9.4 Hz, 1H), 2.10 (s, 3H), 2.08 (s, 3H), 1.28 (t, J = 7.2 Hz, 3H). This was employed for the next step without further purification.

To a solution of diacetate **22** (40 mg, 0.14 mmol) in EtOH (1 mL) was added H_2SO_4 (7.5 μL, 0.14 mmol) and the mixture was stirred for 14 h at room temperature. The reaction was quenched with saturated $NaHCO_3$ aq. solution and organic materials were extracted with EtOAc 10 times. The combined extract was washed with brine, dried over Na_2SO_4, and concentrated *in vacuo*. The residue was purified by preparative TLC [developed with hexane-EtOAc (1:3)] to afforded ethyl shikimate (**1**) as a colorless solid (8.0 mg, 7% over five steps). Its physical properties and spectral data were in good accordance with those of (–)-**1** derived from (+)-**12**.

Acknowledgements

This work was supported by MEXT-Supported Program for the Strategic Research Foundation at Private Universities, 2011–2015. We acknowledge the generous gift of lipases, from Amano Enzyme Inc. for PS-IM, Novozymes Japan for Novozym 435, and Meito Sangyo Co. Ltd. for Meito OF.

Supplementary data

Supplementary data related to this article are provided.

References

1. (a) Abrecht, S.; Harrington, P.; Iding, H.; Karpf, M.; Trussardi, R.; Wirz, B. Zutter, U. *Chimia* **2004**, *58*, 621–629; (b) Shibasaki, M.; Kanai, M.; Yamatsugu, K. *Isr. J. Chem.* **2011**, *51*, 316–328, and references cited therein.
2. For production of shikimic acid, see review; Ghosh, S.; Chisti, Y.; Banerjee, U. C. *Biotech. Adv.* **2012**, *30*, 1425–1431.
3. Draths, K. M.; Knop, D. R.; Frost, J. W. *J. Am. Chem. Soc.* **1999**, *121*, 1603–1604.
4. (a) Adachi, O.; Ano, Y.; Toyama, H.; Matsushita, K. *Biosci. Biotechnol. Biochem.* **2006**, *70*, 2786–2789; (b) Adachi, O.; Ano, Y.; Shinagawa, E.; Yakushi, T.; Matsushita, K. *Biosci. Biotechnol. Biochem.* **2010**, *74*, 2438–2444.
5. (a) Pawlak, J. L.; Berchtold, G. A. *J. Org. Chem.* **1987**, *52*, 1765–1771; (b) Hiroya, K.; Ogasawara, K. *Chem. Commun.* **1998**, 2033–2034; (c) Oritani, T.; Ueda, R.; Kiyota, H. *Biosci. Biotechnol. Biochem.* **2001**, *65*, 2106–2109.
6. (a) Shin, S. H.; Han, J. H.; Lee, S. I.; Ha, Y. B.; Ryu D. H. *Bull. Korean Chem. Soc.* **2011**, *32*, 2885–2886; for *ent*-shikimic acid; (b) Evans, D. A.; Barnes, D. M. *Tetrahedron Lett.* **1997**, *38*, 57–58; (c) Adrio, J.; Carretero, J. C.; Ruano, J. L. G.; Cabrejas, L. M. M. *Tetrahedron: Asymmetry* **1997**, *8*, 1623–1631.
7. Kancharla, P. K.; Doddi, V. R.; Kokatla, H.; Vankar, Y. D. *Tetrahedron Lett.* **2009**, *50*, 6951–6954.
8. Shoji, M.; Imai, H.; Mukaida, M.; Sakai, K.; Kakeya, H.; Osada, H.; Hayashi, Y. *J. Org. Chem.* **2005**, *70*, 79–91.
9. (a) Rakels, J. L. L.; Straathof, A. J. J.; Heijnen, J. J. *Enzyme Microb. Technol.* **1993**, *15*, 1051–1056; (b) Chen, C.-S.; Fujimoto, Y.; Girdaukas, G.; Sih, C. J. *J. Am. Chem. Soc.* **1982**, *104*, 7294–7299.
10. (a) Ema, T. *Curr. Org. Chem.* **2004**, *8*, 1009–1025; (b) Cygler, M.; Grochulski, P.; Kazlauskas, R. J.; Schrag, J. D.; Bouthillier, F.; Rubin, B.; Serreqi, A. N.; Gupta A. K. *J. Am. Chem. Soc.* **1994**, *116*, 3180–3186.
11. Brooks, D. W.; Grothaus, P. G.; Palmer, J. T. *Tetrahedron Lett.* **1982**, *23*, 4187–4190.
12. Nie, L.-D.; Shi, X.-X. *Tetrahedron: Asymmetry* **2009**, *20*, 124–129.
13. Gustin, D. J.; Hilvert, D. *J. Org. Chem.* **1999**, *64*, 4935–4938.

OPEN ACCESS Freely available online

PLOS | ONE

Suppression of Alzheimer's Disease-Related Phenotypes by Geranylgeranylacetone in Mice

Tatsuya Hoshino[1], Koichiro Suzuki[1], Takahide Matsushima[2], Naoki Yamakawa[1], Toshiharu Suzuki[2], Tohru Mizushima[1*]

1 Faculty of Pharmacy, Keio University, Minato-ku, Tokyo, Japan, 2 Graduate School of Pharmaceutical Sciences, Hokkaido University, Sapporo, Hokkaido, Japan

Abstract

Amyloid-β peptide (Aβ) plays an important role in the pathogenesis of Alzheimer's disease (AD). Aβ is generated by the secretase-mediated proteolysis of β-amyloid precursor protein (APP), and cleared by enzyme-mediated degradation and phagocytosis. Transforming growth factor (TGF)-β1 stimulates this phagocytosis. We recently reported that the APP23 mouse model for AD showed fewer AD-related phenotypes when these animals were crossed with transgenic mice expressing heat shock protein (HSP) 70. We here examined the effect of geranylgeranylacetone, an inducer of HSP70 expression, on the AD-related phenotypes. Repeated oral administration of geranylgeranylacetone to APP23 mice for 9 months not only improved cognitive function but also decreased levels of Aβ, Aβ plaque deposition and synaptic loss. The treatment also up-regulated the expression of an Aβ-degrading enzyme and TGF-β1 but did not affect the maturation of APP and secretase activities. These outcomes were similar to those observed in APP23 mice genetically modified to overexpress HSP70. Although the repeated oral administration of geranylgeranylacetone did not increase the level of HSP70 in the brain, a single oral administration of geranylgeranylacetone significantly increased the level of HSP70 when Aβ was concomitantly injected directly into the hippocampus. Since geranylgeranylacetone has already been approved for use as an anti-ulcer drug and its safety in humans has been confirmed, we propose that this drug be considered as a candidate drug for the prevention of AD.

Citation: Hoshino T, Suzuki K, Matsushima T, Yamakawa N, Suzuki T, et al. (2013) Suppression of Alzheimer's Disease-Related Phenotypes by Geranylgeranylacetone in Mice. PLoS ONE 8(10): e76306. doi:10.1371/journal.pone.0076306

Editor: Gianluigi Forloni, "Mario Negri" Institute for Pharmacological Research, Italy

Received March 21, 2013; **Accepted** August 23, 2013; **Published** October 1, 2013

Funding: This work was supported by Grants-in-Aid for Scientific Research from the Ministry of Health, Labour, and Welfare of Japan, as well as the Japan Science and Technology Agency, Grants-in-Aid for Scientific Research from the Ministry of Education, Culture, Sports, Science and Technology, Japan. The funders had no role in study design, data collection and analysis, decision to publish, or preparation of the manuscript.

Competing interests: The authors have declared that no competing interests exist.

* E-mail: mizushima-th@pha.keio.ac.jp

Introduction

Alzheimer's disease (AD) is the most common neurodegenerative disorder and the leading cause of adult-onset dementia. AD is characterized pathologically by the accumulation of neurofibrillary tangles and senile plaques, the latter of which are composed of amyloid-β peptide (Aβ), such as Aβ40 and Aβ42 [1]. To generate Aβ, β-amyloid precursor protein (APP) is first cleaved by β-secretase and then by γ-secretase [2]. γ-secretase is composed of four core components, including presenilin (PS)1 and PS2 [3]. Since early-onset familial AD is linked to three genes, *app, ps1* and *ps2* [3], Aβ is believed to be a key factor in the pathogenesis of AD. Monomeric Aβ easily self-assembles to form oligomers, protofibrils and fibrils, with the oligomers and protofibrils being more neurotoxic than other forms of Aβ [4]. Aβ can be cleared from the brain by different mechanisms such as degradation by enzymes (neprilysin, insulin-degrading enzyme (IDE) and endothelin-converting enzyme (ECE)-2) and phagocytosis by microglia and astrocytes [5]. Therefore, cellular factors that affect the production, self-assembly and clearance of Aβ are likely to offer appropriate targets for the development of drugs to prevent or treat AD.

Inflammation is also important in the pathogenesis of AD [6]. We have previously reported that prostaglandin E_2 (PGE_2), a potent inducer of inflammation, enhances the production of Aβ [7-9], suggesting that inflammation is an aggravating factor for AD. However, as inflammation also activates the Aβ phagocytotic activity of microglia and astrocytes [10], it is evident that the relationship between inflammation and AD progression is complex. Further to the above, transforming growth factor (TGF)-β1, a key cytokine regulating the brain's response to injury and inflammation, was reported to suppress

the progression of AD by stimulating microglial Aβ clearance [10,11].

Cellular up-regulation of expression of heat shock proteins (HSPs), particularly that of HSP70, provides resistance to stressors through the process of refolding or degrading denatured proteins produced by the stressors [12]. Furthermore, several studies have reported that intracellular HSP70 displays anti-inflammatory activity [13,14]. Therefore, HSP70 has received considerable attention for its therapeutic potential. For example, we have shown, using transgenic mice overexpressing HSP70, that HSP70 protects against the development of gastric and small intestine-related lesions, inflammatory bowel disease-related colitis, pulmonary fibrosis and ultraviolet-induced skin damage and hyperpigmentation [15-20].

A number of previous studies have suggested that the expression of HSPs, in particular HSP70, could suppress the progression of AD (see below). Some part of HSPs is secreted into the extracellular space and HSP70 and HSP90 recognize Aβ oligomers and decrease the level of Aβ self-assembly, resulting in the suppression of the production of toxic Aβ [21-23]. Artificial expression of HSP70 protects cultured neurons from Aβ-induced apoptosis [24]. HSP70 stimulates the degradation of APP and Aβ *in vitro* [25], and it has been shown that purified HSP70 and HSP90 activate the phagocytotic activity for Aβ [26]. Furthermore, we showed that crossing APP23 mice (used as an animal model for AD) with transgenic mice overexpressing HSP70 suppresses both the functional and pathological phenotypes. This outcome is probably due to HSP70's activities of anti-aggregation, neuroprotection and stimulation of Aβ clearance [27], and suggests that inducers of HSP70 expression could be good candidates as drugs to treat or inhibit the progression of AD.

Geranylgeranylacetone (GGA), a leading anti-ulcer drug on the Japanese market, has been reported to be a non-toxic HSP-inducer [28]. The HSP-inducing activity of GGA is a major component of its gastro-protective activity [15,17]. Through its cytoprotective, anti-inflammatory and anti-aggregation activities, the induction of HSP70 expression by GGA shows ameliorative effects in animal models of various diseases, such as small intestine-related lesions, inflammatory bowel diseases and pulmonary fibrosis [16,29]. In this study, we examined the effect of GGA on AD phenotypes exhibited by APP23 mice. Orally administered GGA improved not only cognitive deficits displayed by these animals, but also the pathological manifestations associated with these phenotypes.

Materials and Methods

Materials

The fluorescent substrate for β-secretase (H2N-Arg-Glu-(EDANS)-Glu-Val-Asn-Leu-Asp-Ala-Glu-Phe-Lys-(DABCYL)-Arg-OH) was purchased from Calbiochem (Dermstadt, Germany), while fluorescent substrate for γ-secretase (Nma-Gly-Gly-Val-Val-Ile-Ala-Thr-Val-Lys(Dnp)-D-Arg-D-Arg-D-Arg-NH2) and synthetic Aβ42 were from Peptide Institute (Osaka, Japan). Alexa Fluor 488 goat anti-mouse immunoglobulin G was purchased from Invitrogen (Carlsbad, California). Sandwich ELISA kit to detect Aβ oligomers or those to detect Aβ40 and Aβ42 were from Immuno-Biological Laboratories (Fujioka, Japan) or Wako (Osaka, Japan), respectively. The antibody to actin was from Santa Cruz (Santa Cruz, California). Thioflavin-S and antibodies to the C-terminal fragment (CTF) of APP and synaptophysin were from Sigma (St. Louis, Missouri). The antibody to HSP70 was from R&D systems (Minneapolis, MN) and that to PS1 was from Chemicon (Temecula, California). The RNeasy kit was obtained from Qiagen (Valencia, California). The PrimeScript® 1st strand cDNA Synthesis Kit was from TAKARA Bio (Ohtsu, Japan) and SsoFast™ EvaGreen Supermix was from Bio-Rad Laboratories (Hercules, California). Mounting medium for immunohistochemical analysis (VECTASHIELD) was from Vector Laboratories (Burlingame, California). Mounting medium for histological examination (malinol) was purchased from Muto Pure Chemicals (Tokyo, Japan). The Envision kit was from Dako (Carpinteria, California). GGA was purchased from Eisai (Tokyo, Japan).

Animals and Drug administration

APP23 mice (C57BL/6 mice expressing mutant APP (Swedish type)) were a gift from Dr. M Staufenbiel (Novartis Institutes for BioMedical Research, Basel, Switzerland) [30]. All experiments in this study were performed using littermate female mice (heterogeneous APP23 and wild-type mice).

For repeated oral administration of GGA to mice, we used GGA-supplemented chow. GGA granules were mixed with powdered rodent chow at a concentration of 1%. On the assumption that the average mouse weighs 24 g and consumes 3 g of chow per day, this dose was predicted to supply 1.25 g GGA per kg body weight per day. The actual average dose of GGA was calculated to be 1.76 g per kg body weight per day based on the amount of chow taken. The LD_{50} value of GGA (a dose causing 50% survival rate) in mice was reported to be more than 15 g per kg body weight [31].

For the single oral administration of GGA to mice, GGA was dissolved in 5% gum Arabic and 0.06% Tween and administered orally (500 mg/kg, 10 ml/kg).

The experiments and procedures described here were carried out in accordance with the Guide for the Care and Use of Laboratory Animals as adopted and promulgated by the National Institutes of Health, and were approved by the Animal Care Committee of Keio University (Permit Number: 12001-0). All surgery was performed under sodium pentobarbital anesthesia, and all efforts were made to minimize suffering.

Preparation and Injection of Aβ42 oligomers

Oligomerized Aβ42 was prepared as described previously [32], with minor modifications. Aβ42 peptides were dissolved in 1, 1, 1, 3, 3, 3-hexafluoro-2-propanol, dried and stored. The dried peptides were dissolved in anhydrous DMSO at 100 mM and diluted in saline to give a final concentration of 100 μM. After 16 h incubation at 22°C, the preparation was centrifuged at 21, 000 x g for 15 min and the supernatant was used for experiments.

For the injection of Aβ42 oligomers, mice were anaesthetized with pentobarbital sodium. Bilateral stereotaxic injection of

Aβ42 oligomers (1 μl, 100 pmol) or saline (sham) into the hippocampus (AP -2.5mm, L +/-2.0 mm, DV -1.5 mm) was performed using a Hamilton syringe. The injection speed was 0.5 μl/min and the needle was maintained in place for an additional 2 min before being slowly withdrawn. The dose and procedures for the injection were determined based on previous papers [33,34].

Immunoblotting Analysis

Whole cell extracts were prepared as described previously [27]. The protein concentration of each sample was determined by the Bradford method. Samples were applied to SDS polyacrylamide gels (Tris/tricine gels for the detection of CTFα and CTFβ, and Tris/glycine gels for the detection of other proteins) and subjected to electrophoresis, after which proteins were immunoblotted with each antibody.

Real-time RT-PCR Analysis

Real-time RT-PCR was performed as described previously [27], with some modifications. Total RNA was extracted from the brain using an RNeasy kit according to the manufacturer's protocol. Samples (1 μg RNA) were reverse-transcribed using a first-strand cDNA synthesis kit. Synthesized cDNA was used in real-time RT-PCR (Chromo 4 instrument, Bio-Rad Laboratories) experiments using SsoFast™ EvaGreen Supermix, and then analyzed with Opticon Monitor Software. Specificity was confirmed by electrophoretic analysis of the reaction products and by inclusion of template- or reverse transcriptase-free controls. To normalize the amount of total RNA present in each reaction, glyceraldehyde-3-phosphate dehydrogenase (GAPDH) cDNA was used as an internal standard.

Primers were designed using the Primer3 website. The primers used were (name: forward primer, reverse primer): *gapdh*: 5'-aactttggcattgtggaagg-3', 5'-acacattgggggtaggaaca-3'; *neprilysin*: 5'-gcagcctcagccgaaactac-3', 5'-caccgtctccatgttgcagt-3'; *ide*: 5'-accaggaaatgttggctgtc-3', 5'-tctgagaggggaactctcca-3'; *ece-2*: 5'-gctatgcccatgtacccagt-3', 5'-tggcatccagagtaccttc-3'; *il-1β*: 5'-gatcccaagcaatacccaaa-3', 5'-ggggaactctgcagactcaa-3'; *il-6*: 5'-ctggagtcacagaaggagtgg-3', 5'-ggtttgccgagtagatctcaa-3'; *tnf-α*: 5'-cgtcagccgatttgctatct-3', 5'-cggactccgcaaagtctaag-3'; *tgf-β1*: 5'-tgacgtcactggagtacgg-3', 5'-ggttcatgtcatggatggtgc-3'.

Morris Water Maze Test

The Morris water maze test was conducted in a circular 90 cm diameter pool filled with water at 22.0 ± 1°C, as described previously [9]. In the hidden platform test, a circular platform (10 cm in diameter) was submerged 0.5 cm below water level. Swimming paths were tracked for 60 s with a camera, and stored in a computer (Video Tracking System CompACT VAS/DV, Muromachi Kikai, Tokyo, Japan). The mice were given 4 trials (1 block) per day for 7 consecutive days, during which the platform was left in the same position. The time taken to reach the platform (escape latency) was measured and the average time for the 4 trials was determined.

Twenty-four hours after the last trial of the hidden platform test, the mice were subjected to a transfer test in which the platform was removed, and their swimming path was recorded for 60 s. Percent search time for each quadrant and crossing time in the area where the platform had been located were determined.

Sandwich ELISA (sELISA) for Aβ

Aβ40 and Aβ42 levels in the brain were determined as described previously [35]. Briefly, the brain hemispheres were homogenized in 50 mM Tris/HCl buffer (pH 7.6) containing 150 mM NaCl, and then centrifuged. Guanidine/HCl (0.5 M, final concentration) was added to the supernatants (soluble fractions). The precipitates were solubilized by sonication in 6 M guanidine/HCl, after which the solubilized pellet was centrifuged to obtain supernatants (insoluble fractions). The amounts of Aβ40 and Aβ42 in each fraction were determined by sELISA according to the manufacturer's instructions (Wako). An ELISA assay for Aβ oligomers was carried out on the soluble fractions (but without guanidine/HCl) according to the manufacturer's instructions (Immuno-Biological Laboratories).

Thioflavin-S Staining and Immunohistochemical Analyses

Brain hemispheres were fixed in 4% buffered paraformaldehyde and embedded in paraffin before being cut into 4 μm-thick sections, which were then deparaffinized and washed in phosphate-buffered saline. Sections were prepared from the coronal plane and images were carefully matched for location in the rostral-caudal (2.0 mm posterior to bregma) directions. Observers were blinded to conditions in all experiments. For statistical analysis, we used three sections (every 10 sections) per mouse and calculated an average value for the three sections. The *n* value reported in each figure indicates the number of mice used for experiments.

For thioflavin-S staining, sections were stained with a 1% thioflavin-S solution. Samples were mounted with malinol and inspected using a BX51 microscope (Olympus, Tokyo, Japan). Fluorescence microscope images of regions (1.0 mm^2) in the hippocampus or cerebral cortex were used to calculate the area stained with thioflavin-S; this was done using LuminaVision software (Mitani, Fukui, Japan). Using the threshold optical density, we divided the total area under consideration into thioflavin-S-positive and negative areas and determined the thioflavin-S-positive area as a percentage of the total area.

For immunohistochemical analysis to detect synaptophysin, sections were blocked with 2.5% goat serum for 10 min, incubated for 12 h with antibody to synaptophysin (1:200 dilution) in the presence of 2.5% bovine serum albumin, and then incubated with Alexa Fluor 488 goat anti-mouse immunoglobulin G. Samples were mounted with VECTASHIELD and inspected with the aid of a BX51 fluorescence microscope. Fluorescence intensity in a 100 μm x 150 μm area of the hippocampal CA3 region was determined using LuminaVision software and expressed relative to the fluorescence intensity measured in the same region in wild-type mice.

β- and γ-secretase-mediated Peptide Cleavage Assay

β- and γ-secretase activity was monitored as reported previously [9]. Solubilized membranes were incubated for 1 h at 37°C in 200 µl of 50 mM acetate buffer (pH 4.1) containing 100 mM sodium chloride, 0.025% bovine serum albumin and 10 µM β-secretase fluorescent substrate, or for 4 h at 37°C in 200 µl of 50 mM Tris/HCl buffer (pH 6.8) containing 2 mM EDTA, 0.25% CHAPSO and 10 µM γ-secretase fluorescent substrate. Fluorescence was measured using a plate reader (Fluostar Galaxy, BMG Labtechnologies, Offenburg, Germany) with an excitation wavelength of 355 nm and an emission wavelength of 510 nm (for β-secretase) or 440 nm (for γ-secretase).

Statistical Analysis

All values are expressed as the mean ± SEM. One- or two-way analysis of variance (ANOVA) followed by the Tukey test was used to evaluate differences between more than three groups. The Student's *t*-test for unpaired results was used for the evaluation of differences between two groups. Differences were considered to be significant for values of $P<0.05$. The *P* value or *F* value of the ANOVA analysis are shown in the text.

Results

Effect of orally administered GGA on cognitive function in APP23 mice

To examine the effect of GGA on APP23 mice at 12 months of age when AD-related phenotypes become apparent, we selected the administration period (9 months) and dosage (chow containing GGA at a concentration of 1%) based on a previous report [36]. The Morris water maze test was used to examine spatial learning and memory. APP23 and wild-type (C57BL/6) mice were fed either GGA-supplemented chow or control chow from the age of 3 months to 12 months and spatial learning and memory was tested at the end of this period (n=13 for WT-Control, n=11 for WT-GGA, n=15 for APP23-Control, and n=15 for APP23-GGA). No significant differences among the four groups of mice (APP23 or wild-type mice fed GGA-supplemented or control chow) were observed in terms of the amounts of chow consumed, in swimming speed or in ability to locate a visible platform (data not shown). Mice were trained 4 times per day for 7 days to learn the location of a hidden platform, and the time required to reach the platform (escape latency) was measured. As shown Figure 1A, APP23 mice fed control chow took a significantly longer time than wild-type mice on the same diet to reach the platform, confirming that APP23 mice have a deficiency in spatial learning and memory. APP23 mice fed GGA-supplemented chow took a significantly shorter time to find the hidden platform than their counterparts fed the control chow (Figure 1A). In contrast, GGA administration did not affect the escape latency in wild-type mice (Figure 1A) (two-way repeated measures ANOVA, genotype effect $F_{(1, 50)}$=5.42, P=0.021; GGA effect $F_{(1, 50)}$=4.92, P=0.031; interaction $F_{(1, 50)}$= 4.09, P=0.048).

We next performed a transfer test to estimate the spatial memory of platform location. Following a 7-day training period

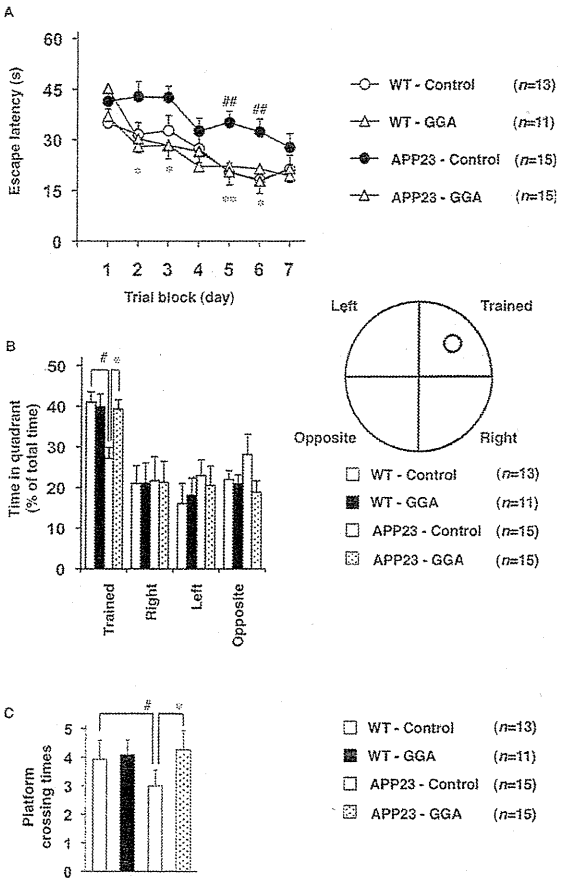

Figure 1. Effects of oral administration of GGA on spatial learning and memory in APP23 mice. Cognitive behavioral tests using the Morris water maze were carried out on 12-month-old wild-type (WT) and APP23 mice fed either GGA-supplemented chow (10 g GGA/kg chow) or control chow from 3 to 12 months of age as described in the experimental procedures. The average escape latency in each trial block (4 tests) was measured for 7 days (A), after which the mice were subjected to a transfer test in which the platform was removed. The spatial memory test for platform location was estimated by the percent search time spent in each quadrant (the platform had been located in the "trained" quadrant) (B) or platform crossing times (C). Values are given as mean ± SEM (n=13 for WT-Control, n=11 for WT-GGA, n=15 for APP23-Control, and n=15 for APP23-GGA). **P <0.01 and *P <0.05, APP23-GGA versus APP23-Control; ##P <0.01 and # P <0.05, APP23-Control versus WT-Control.

doi: 10.1371/journal.pone.0076306.g001

(see above), each mouse was subjected to a Morris water maze test in which the platform was removed and the percent search time for each quadrant was measured. As shown in Figure 1B, the ratio of time spent in the trained quadrant was lower for the APP23 mice fed control chow compared not only

with wild-type mice fed control chow but also with APP23 mice fed GGA-supplemented chow (Figure 1B) (Two-way ANOVA, genotype effect $F_{(1, 50)}$=6.11, P=0.017; GGA effect $F_{(1, 50)}$=3.87, P=0.055; interaction $F_{(1, 50)}$=5.36, P=0.025). The crossing time of the area where the platform had been located, another indicator of spatial memory, was lower for the APP23 mice fed control chow compared with wild-type mice fed control chow and APP23 mice fed GGA-supplemented chow (Figure 1C) (two-way ANOVA, genotype effect $F_{(1, 50)}$=3.64, P=0.062; GGA effect $F_{(1, 50)}$=7.97, P=0.007; interaction $F_{(1, 50)}$=5.76, P=0.020). GGA administration did not affect these indexes in wild-type mice (Figure 1B and C). These results suggest that the deficit in spatial learning and memory in APP23 mice was ameliorated by the oral administration of GGA.

Effect of orally administered GGA on Aβ levels, Aβ accumulation and synaptic loss in APP23 mice

We have previously reported that genetic overexpression of HSP70 decreases levels of Aβ, Aβ plaque deposition and synaptic loss in mice [27]. In the present study, we examined whether similar alteration could be observed in APP23 mice administered GGA. Levels of Aβ40 and Aβ42 in both soluble and insoluble brain fractions were lower in APP23 mice fed GGA-supplemented chow than for those fed control chow (Figure 2A) (Student's *t*-test, soluble Aβ40, P=0.046; soluble Aβ42, P=0.040; insoluble Aβ40, P=0.036; insoluble Aβ42, P=0.038). Similar results were observed with regard to the level of Aβ oligomers (Figure 2B) (n=8 for APP23-Control and n=7 for APP23-GGA) (Student's *t*-test, P =0.011).

We next examined the effects of orally administered GGA on Aβ plaque deposition and neurotoxicity, which were reported to occur in APP23 mice [37]. Thioflavin-S staining revealed that the level of Aβ plaque deposition in the cerebral cortex was lower in APP23 mice fed GGA-supplemented chow than in those fed control chow (Figure 2C and D) (n=5 for WT-Control, n=5 for WT-GGA, n=8 for APP23-Control, and n=7 for APP23-GGA) (Figure 2D, upper panel, two-way ANOVA, genotype effect $F_{(1, 21)}$=40.34, P<0.001; GGA effect $F_{(1, 21)}$=10.49, P=0.004; interaction $F_{(1, 21)}$=5.42, P=0.030). We could not detect to any significant extent the deposition of Aβ plaque in the hippocampus of APP23 mice at 12 months of age (Figure 2C and D) (Figure 2D, lower panel, two-way ANOVA, genotype effect $F_{(1, 21)}$=0.25, P=0.620; GGA effect $F_{(1, 21)}$=0.42, P=0.524; interaction $F_{(1, 21)}$=0.14, P=0.710).

We also estimated the number of synapses based on synaptophysin staining and found that the level of staining was higher in sections from APP23 mice fed the GGA-supplemented chow compared with those fed control chow (Figure 2E and F) (n=5 for WT-Control, n=5 for WT-GGA, n=8 for APP23-Control, and n=7 for APP23-GGA) (two-way ANOVA, genotype effect $F_{(1, 21)}$=7.84, P=0.011; GGA effect $F_{(1, 21)}$=6.03, P=0.023; interaction $F_{(1, 21)}$=6.81, P=0.016). These results suggest that synaptic loss was ameliorated by the administration of GGA. All results in Figure 2 suggest that the oral administration of GGA decreases the level of Aβ (monomer and oligomers) and Aβ plaque deposition in the brain and protects neurons against Aβ-induced neurotoxicity.

Effect of orally administered GGA on the production of Aβ and on the expression of genes involving Aβ clearance

In general, the production of Aβ is regulated either by the modification of APP or by the modulation of secretase activity. To this extent, we recently reported that the genetic overexpression of HSP70 in mice affects neither the modification of APP nor secretase activity [27]. Here we examined the effects of orally administered GGA on the modification of APP and secretase activity in APP23 mice. The mature (*N*- and *O*-glycosylated) and immature (*N*-glycosylated alone) forms of APP (mAPP and imAPP, respectively) can be differentiated by using SDS-PAGE. As shown in Figure 3A, the total amount of APP and the ratio of mAPP to imAPP in whole cell extracts prepared from the brains of 12-month-old wild-type and APP23 mice were not affected by the oral administration of GGA (Student's *t*-test, P =0.48). We also found that the same treatment did not affect the level of PS1 (Figure 3A) (n=3 for APP23-Control and n=3 for APP23-GGA) (Student's *t*-test, P =0.34).

The secreted forms of APP generated by α and β-secretase are CTFα and CTFβ, respectively, which can be used as an indirect index of the secretase activity. As shown in Figure 3B, the relative amounts of CTFα and CTFβ were not affected by the administration of GGA to animals (Student's *t*-test, CTFα, P =0.12; CTFβ, P =0.42). Under our experimental conditions, the CTFγ band could not be detected (data not shown). We also measured β- and γ-secretase activity directly, using the APP-derived fluorescent substrate. As shown in Figure 3C, the activities of these enzymes were indistinguishable between APP23 mice fed GGA-supplemented chow and those fed control chow (n=8 for APP23-Control and n=7 for APP23-GGA) (Student's *t*-test, β-secretase, P =0.48; γ-secretase, P =0.14). The results in Figure 3 thus suggest that the oral administration of GGA does not affect Aβ production.

As described in the Introduction, Aβ degradation by enzymes and Aβ phagocytosis by microglia and astrocytes are involved in the clearance of Aβ [5]. We recently reported that the genetic overexpression of HSP70 affects the expression of genes involved in these processes (*ide* and *tgf-β1*), leading us to examine here the effects of orally administered GGA on the mRNA expression of these genes. Real-time RT-PCR analysis revealed that orally administered GGA up-regulated the expression of *ide* and *tgf-β1* but did not affect the expression levels of the other genes tested (*neprilysin*, *ece-2*, *il-1β*, *il-6* and *tnf-α*) (Figure 4) (n=6 for APP23-Control and n=6 for APP23-GGA) (Student's *t*-test, *ide*, P=0.013; *tgf-β1*, P=0.011; *neprilysin*, P=0.29; *ece-2*, P=0.46; *il-1β*, P=0.17; *il-6*, P=0.49; *tnf-α*, P=0.44). These results suggest that, as for the genetic overexpression of HSP70, orally administered GGA also decreases Aβ levels, at least partly, through the up-regulation of *ide* and *tgf-β1* expression.

Effects of orally administered GGA on HSP70 expression in the brain

Finally, we examined the effect of orally administered GGA on the expression of HSP70 in the brain under conditions in which alterations of functional and pathological phenotypes in

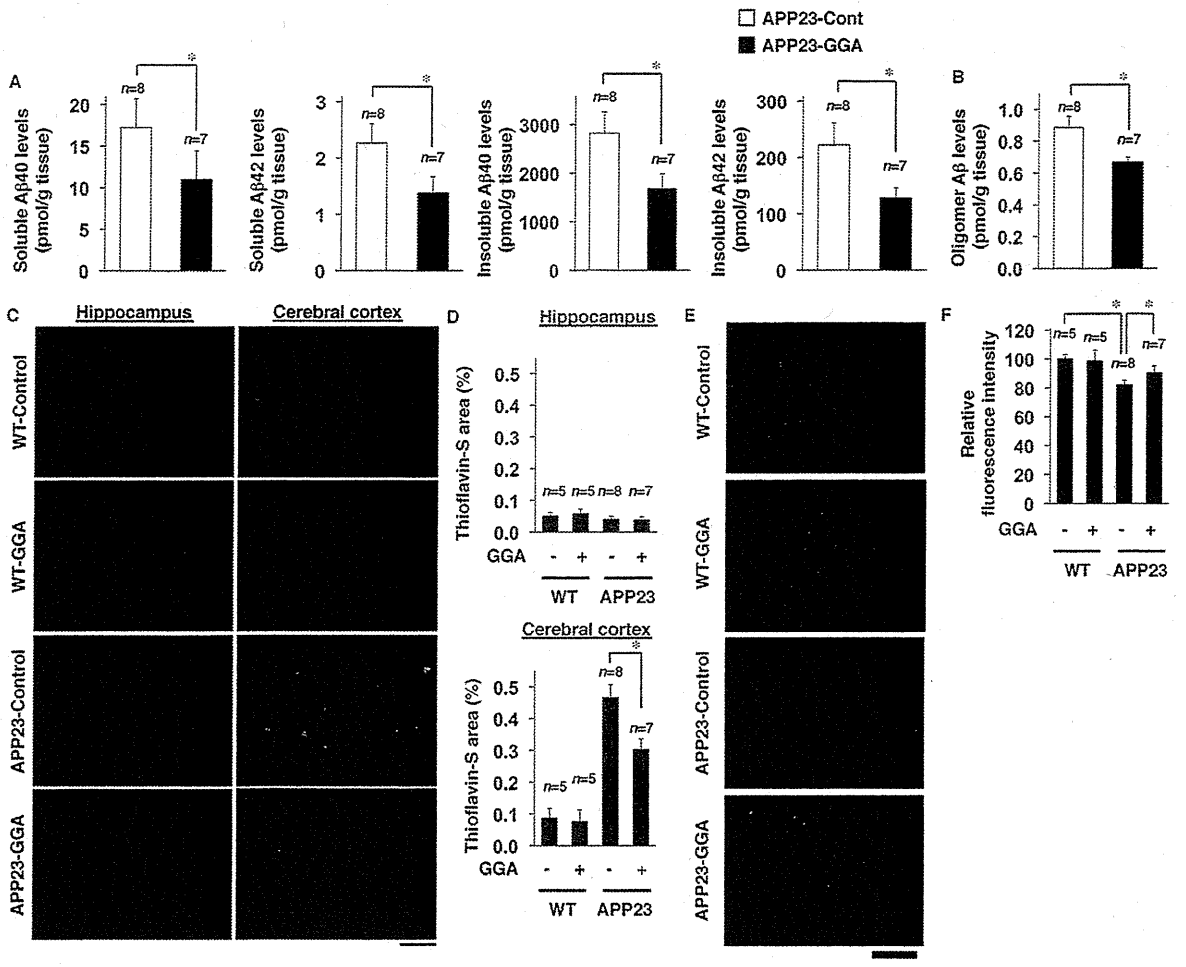

Figure 2. Effects of orally administered GGA on Aβ levels and synaptic loss. Soluble and insoluble fractions and sections were prepared from the whole brains of 12-month-old wild-type mice (WT) and APP23 mice fed either GGA-supplemented chow or control chow (see the legend of Figure 1). The amounts of Aβ40 and Aβ42 in each fraction or Aβ oligomers in the soluble fraction were determined by sELISA as described in the experimental procedures (A, B). Brain sections were subjected to thioflavin-S staining (scale bar, 200 μm) (C) or immunohistochemical analysis with an antibody to synaptophysin (scale bar, 50 μm) (E). The percentage of area stained with thioflavin-S in the hippocampus or cerebral cortex (D), or the relative fluorescence intensity (synaptophysin) in the hippocampal CA3 region (F) was determined. Three sections were prepared from each mouse and their average was calculated (D, F). Values are given as mean ± SEM (n=5 for WT-Control, n=5 for WT-GGA, n=8 for APP23-Control, and n=7 for APP23-GGA). **P<0.01; *P<0.05.

doi: 10.1371/journal.pone.0076306.g002

APP23 mice were observed (GGA administration from the age of 3 to 12 months). As shown in Figure 5A and B, this regime of GGA administration did not affect the expression of HSP70 in either APP23 or wild-type mice at the age of 12 months (n=5 for WT-Control, n=5 for WT-GGA, n=6 for APP23-Control, and n=6 for APP23-GGA) (Figure 5B) (two-way ANOVA, genotype effect $F_{(1, 18)}$=0.01, P=0.912; GGA effect $F_{(1, 18)}$=0.23, P=0.635; interaction $F_{(1, 18)}$=0.07, P=0.794). We therefore examined the effect of oral GGA administration on the expression of HSP70 under other conditions. First, we considered the possibility that GGA might up-regulate the expression of HSP70 in younger mice (i.e. 3 months old) but not in older ones (i.e. 12 months old) and examined the expression of HSP70 in 4-month-old mice after a 1-month period of oral administration of GGA. As shown in Figure 5C and D, although there was a tendency for GGA to increase the expression of HSP70 in the brain under these conditions, the result was not statistically significant (n=6 for WT-Control, n=6 for WT-GGA, n=5 for APP23-Control, and n=5 for APP23-GGA) (Figure 5D) (two-way ANOVA, genotype effect $F_{(1, 18)}$=6.11, P=0.024; GGA effect $F_{(1, 18)}$=0.29, P=0.598;

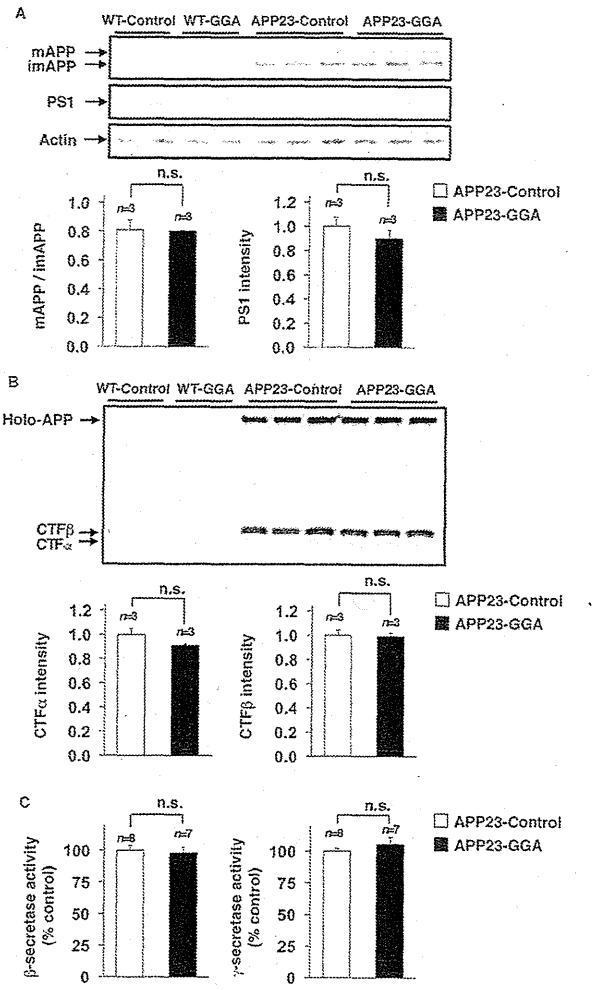

Figure 3. Effects of orally administered GGA on APP maturation and secretase activity. Whole cell extracts or membrane fractions were prepared from the brains of 12-month-old wild-type (WT) and APP23 mice fed either GGA-supplemented chow or control chow (see the legend of Figure 1). Whole cell extracts were subjected to immunoblotting with an antibody to APP (A, B), PS1 (A) or actin (A). The band intensity ratio (mAPP/imAPP) was determined (A). The band intensity of PS1, CTFα and CTFβ was determined, corrected with that of actin (PS1) or holo-APP (CTFα and CTFβ) (A, B) (n=3 for APP23-Control and n=3 for APP23-GGA). Membrane fractions were subjected to a β- or γ-secretase-mediated peptide cleavage assay as described in the experimental procedures (C) (n=8 for APP23-Control and n=7 for APP23-GGA). Values are given as mean ± SEM. n.s., not significant.

doi: 10.1371/journal.pone.0076306.g003

interaction $F_{(1,\ 18)}$=0.04, P=0.839). We then considered that GGA might require more stressful conditions to up-regulate the expression of HSP70. On this basis, we examined the effect of

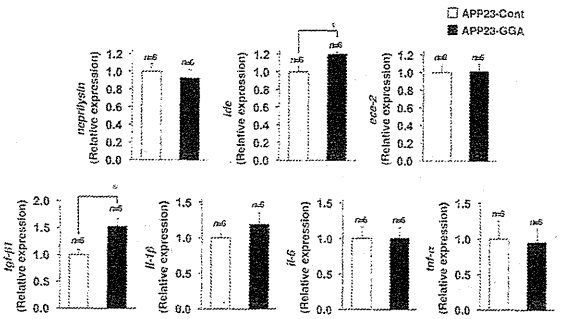

Figure 4. Effects of orally administered GGA on the expression of Aβ-degrading enzymes and cytokines. Total RNA was extracted from the brains of 12-month-old APP23 mice fed either GGA-supplemented chow or control chow (see the legend of Figure 1). Samples were subjected to real-time RT-PCR using a specific primer for each gene. Values were normalized to *gapdh* gene expression and expressed relative to the control sample. Values are given as mean ± SEM (n=6 for APP23-Control and n=6 for APP23-GGA). *P<0.05.

doi: 10.1371/journal.pone.0076306.g004

orally administered GGA and/or the bilateral injection of Aβ42 oligomers into the hippocampus on the expression of HSP70 in this region. As shown in Figure 5E and F, the GGA significantly increased the expression of HSP70 in the brain when Aβ42 oligomers was concomitantly injected into the hippocampal region. The oral administration of GGA, or the injection of Aβ42 oligomers alone, both showed a tendency to increase the expression of HSP70; however, the increase was not statistically significant (Figure 5E and F) (n=10 for Sham-Vehicle, n=8 for Sham-GGA, n=12 for Aβ-Vehicle, and n=11 for Aβ-GGA) (Figure 5F) (two-way ANOVA, Aβ injection effect $F_{(1,\ 37)}$=10.32, P=0.003; GGA effect $F_{(1,\ 37)}$=45.15, P<0.001; interaction $F_{(1,\ 37)}$= 4.11, P=0.048). These results suggest that orally administered GGA could up-regulate the expression of HSP70 in the brain in the presence of elevated levels of Aβ oligomers.

Discussion

As outlined in the Introduction, numerous beneficial effects of HSP70 in animal models of various diseases have been reported. With respect to a range of neurodegenerative diseases, the overexpression of HSP70 has been shown to suppress the aggregation of pathogenic proteins and to ameliorate the corresponding disease symptoms [22,27,36,38]. Such findings give rise to the notion of the potential benefits of HSP70 inducers to retard or inhibit the progression of neurodegenerative diseases. It was reported that orally administered GGA ameliorates disease symptoms in an animal model of spinal and bulbar muscular atrophy [36] and we here examined the effect of GGA on the phenotypes exhibited by an animal model of AD.

It was previously reported that GGA achieves its anti-ulcer activity after absorption by the intestinal mucosa and also that

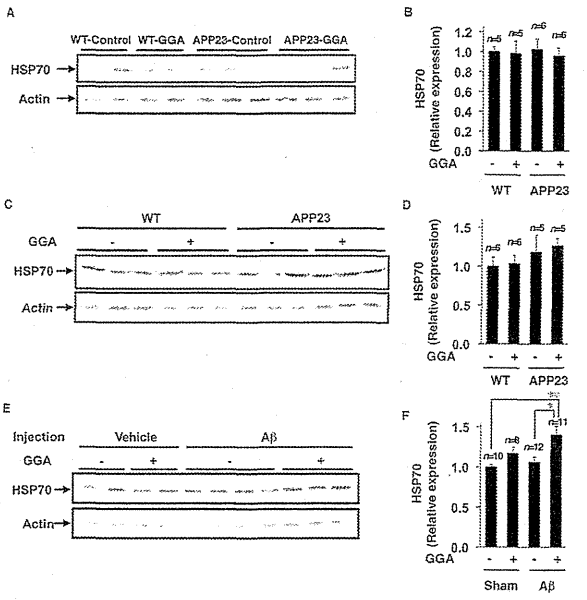

Figure 5. Effects of orally administered GGA and/or injection of Aβ42 oligomers on the expression of HSP70. Wild-type (WT) and APP23 mice were fed either GGA-supplemented chow (10 g GGA/kg chow) or control chow from the age of 3 months to 12 months (A, B) (n=5 for WT-Control, n=5 for WT-GGA, n=6 for APP23-Control, and n=6 for APP23-GGA) or from the age of 3 months to 4 months (C, D) (n=6 for WT-Control, n=6 for WT-GGA, n=5 for APP23-Control, and n=5 for APP23-GGA). Whole cell extracts were prepared from the brains of 12-month-old mice (A, B) or 4-month-old mice, respectively (C, D). Three-month-old wild-type mice were given a once only orally administered dose of 500 mg/kg of GGA, and 3 h later Aβ42 oligomers (1 μl, 100 pmol) was injected into the hippocampus. Whole cell extracts were prepared from the hippocampus 24 h after the injection (E, F) (n=10 for Sham-Vehicle, n=8 for Sham-GGA, n=12 for Aβ-Vehicle, and n=11 for Aβ-GGA). Samples were subjected to immunoblotting with an antibody to HSP70 or actin (A, C, E). The band intensity of HSP70 was determined, corrected to that of actin and expressed relative to the control (B, D, F). Values are given as mean ± SEM. $^{**}P<0.01$; $^{*}P<0.05$.

doi: 10.1371/journal.pone.0076306.g005

GGA is able to pass through blood brain barrier [39,40]. These findings suggest that GGA could be administered orally to up-regulate the expression of HSPs in the brain. To this extent, in the animal model of spinal and bulbar muscular atrophy mentioned above, the up-take of GGA incorporated in chow (1%) induced the expression of HSP70 in the spinal cord and ameliorated the neuromuscular symptoms displayed by these animals [36]. Moreover, in an animal model of focal cerebral ischemia, orally administered GGA (1000 mg/kg) induced the expression of HSP70 in the brain and reduced the infarct volume [41], while in an experimental intracerebral hemorrhage model, orally administered GGA (800 mg/kg) induced the expression of HSP70 and reduced the extent of hemorrhage [42]. It should be noted that in all these previous reports, the GGA-induced expression of HSP70 was observed in the disease models but not so clearly in control animals. It could thus be interpreted that GGA may enhance the expression of HSP70 induced by other stressors in the brain.

We showed that orally administered GGA improved not only cognitive function (spatial learning and memory) but also reduced the pathological phenotypes (reducing levels of Aβ (monomer and oligomers), Aβ plaque deposition and synaptic loss) exhibited by APP23 mice. We also found that the orally administered GGA did not alter APP maturation or secretase activity in the brain; however the expression of *ide* and *tgf-β1* was up-regulated by this treatment protocol. All these phenomena are similar to those observed in APP23 mice crossed with transgenic mice overexpressing HSP70 [27], suggesting that GGA achieves these ameliorative effects through the up-regulation of HSP70 expression in the brain. In other words, we consider that HSP70's abilities to unfold and refold Aβ aggregates, to protect against Aβ neurotoxicity, to suppress inflammation and to stimulate Aβ clearance are involved in these ameliorative effects of GGA. However, it should be noted that the extent of amelioration was not so apparent in APP23 mice fed GGA-supplemented chow as in those crossed with transgenic mice expressing HSP70 [27], possibly reflecting the higher level of HSP70 expression in the latter mice.

Surprisingly, orally administered GGA (from the age of 3 to 12 months) did not affect the expression of HSP70 at the brain level even in APP23 mice at the age of 12 months. It was reported that in an animal model of Huntington's disease, the induction of HSP70 became less apparent as the disease progressed [43]. Thus, considering the possibility that GGA could up-regulate HSP70 expression in younger mice, we examined HSP70 expression in 4-month-old animals after a 1-month period of oral administration of GGA. Although we identified a tendency for this treatment to increase HSP70 expression in the brain, the level of alteration was not statistically significant. We then considered that GGA might up-regulate the expression of HSP70 only in the region confined to where toxic Aβ levels are high, or that Aβ's neurotoxicity might be so weak that the GGA-dependent up-regulation of HSP70 expression might be undetectable by the immunoblot assay technique. In any case, we predicted that a large increase in Aβ neurotoxicity would cause the GGA-dependent up-regulation of HSP70 expression to become clearly apparent. Indeed, in the presence of Aβ42 oligomers injected directly into the hippocampus, concomitantly administered GGA significantly increased the expression of HSP70.

We cannot be certain at this point in time whether GGA achieves its ameliorative effects on AD-related phenotypes in APP23 mice through its HSP-inducing activity. To this extent, it is possible that GGA achieves its ameliorative effects through HSP-independent mechanisms. Various pharmacological activities of GGA other than HSP-inducing activity have been reported [44,45]. GGA was originally developed as an anti-ulcer drug based on its capacity to increase gastric mucosal blood flow and mucus production [46,47]. We previously

reported that GGA protects membranes against NSAID-induced permeabilization [48], and it was recently reported that GGA inhibits replication of the hepatitis C virus through either an inhibitory effect on the geranylgeranylation of proteins or on the activation of mTOR [49,50]. Thus, we cannot rule out the possibility that such HSP-independent pharmacological activities might be involved in the ameliorative effects of GGA on AD-related phenotypes in APP23 mice. Even so, it would be difficult to reconcile such pharmacological activities with the noted improvements in cognitive function, Aβ plaque deposition, synaptic loss, Aβ clearance, Aβ phagocytosis and so on.

Although the molecular mechanism of GGA's action is not clear at present, the results of this study suggest that GGA could be a candidate for use as a new type of anti-AD drug. A number of new compounds are being developed for this purpose; however, as the development of new molecules requires an enormous economic commitment by drug companies and the distinct possibility exists of encountering unacceptable side effects in late-stage clinical trials. GGA might offer a distinct advantage given that its safety has already been clinically demonstrated.

Acknowledgements

We thank Dr. M Staufenbiel (Novartis Institutes for BioMedical Research) for providing transgenic mice.

Author Contributions

Conceived and designed the experiments: T. Mizushima TH TS. Performed the experiments: TH KS. Analyzed the data: TH KS. Contributed reagents/materials/analysis tools: T. Matsushima NY. Wrote the manuscript: T. Mizushima.

References

1. Hardy J, Selkoe DJ (2002) The amyloid hypothesis of Alzheimer's disease: progress and problems on the road to therapeutics. Science 297: 353-356. doi:10.1126/science.1072994. PubMed: 12130773.
2. Selkoe DJ (1999) Translating cell biology into therapeutic advances in Alzheimer's disease. Nature 399: A23-A31. doi:10.1038/399a023. PubMed: 10392577.
3. Haass C (2004) Take five--BACE and the gamma-secretase quartet conduct Alzheimer's amyloid beta-peptide generation. EMBO J 23: 483-488. doi:10.1038/sj.emboj.7600061. PubMed: 14749724.
4. Haass C, Selkoe DJ (2007) Soluble protein oligomers in neurodegeneration: lessons from the Alzheimer's amyloid beta-peptide. Nat Rev Mol Cell Biol 8: 101-112. doi:10.1038/nrm2101. PubMed: 17245412.
5. Miners JS, Baig S, Palmer J, Palmer LE, Kehoe PG et al. (2008) Abeta-degrading enzymes in Alzheimer's disease. Brain Pathol 18: 240-252. doi:10.1111/j.1750-3639.2008.00132.x. PubMed: 18363935.
6. Wyss-Coray T (2006) Inflammation in Alzheimer disease: driving force, bystander or beneficial response? Nat Med 12: 1005-1015. PubMed: 16960575.
7. Hoshino T, Namba T, Takehara M, Nakaya T, Sugimoto Y et al. (2009) Prostaglandin E2 stimulates the production of amyloid-beta peptides through internalization of the EP4 receptor. J Biol Chem 284: 18493-18502. doi:10.1074/jbc.M109.003269. PubMed: 19407341.
8. Hoshino T, Nakaya T, Homan T, Tanaka K, Sugimoto Y et al. (2007) Involvement of prostaglandin E2 in production of amyloid-beta peptides both in vitro and in vivo. J Biol Chem 282: 32676-32688. doi:10.1074/jbc.M703087200. PubMed: 17767011.
9. Hoshino T, Namba T, Takehara M, Murao N, Matsushima T et al. (2012) Improvement of cognitive function in Alzheimer's disease model mice by genetic and pharmacological inhibition of the EP(4) receptor. J Neurochem 120: 795-805. doi:10.1111/j.1471-4159.2011.07567.x. PubMed: 22044482.
10. Wyss-Coray T, Lin C, Yan F, Yu GQ, Rohde M et al. (2001) TGF-beta1 promotes microglial amyloid-beta clearance and reduces plaque burden in transgenic mice. Nat Med 7: 612-618. doi:10.1038/87945. PubMed: 11329064.
11. Tesseur I, Zou K, Esposito L, Bard F, Berber E et al. (2006) Deficiency in neuronal TGF-beta signaling promotes neurodegeneration and Alzheimer's pathology. J Clin Invest 116: 3060-3069. doi:10.1172/JCI27341. PubMed: 17080199.
12. Liberek K, Lewandowska A, Zietkiewicz S (2008) Chaperones in control of protein disaggregation. EMBO J 27: 328-335. doi:10.1038/sj.emboj.7601970. PubMed: 18216875.
13. Sun D, Chen D, Du B, Pan J (2005) Heat shock response inhibits NF-kappaB activation and cytokine production in murine Kupffer cells. J Surg Res 129: 114-121. doi:10.1016/j.jss.2005.05.028. PubMed: 16243048.
14. Chan JY, Ou CC, Wang LL, Chan SH (2004) Heat shock protein 70 confers cardiovascular protection during endotoxemia via inhibition of nuclear factor-kappaB activation and inducible nitric oxide synthase expression in the rostral ventrolateral medulla. Circulation 110: 3560-3566. doi:10.1161/01.CIR.0000143082.63063.33. PubMed: 15557375.
15. Tanaka K, Tsutsumi S, Arai Y, Hoshino T, Suzuki K et al. (2007) Genetic evidence for a protective role of heat shock factor 1 against irritant-induced gastric lesions. Mol Pharmacol 71: 985-993. doi: 10.1124/mol.106.033282. PubMed: 17189318.
16. Asano T, Tanaka K, Yamakawa N, Adachi H, Sobue G et al. (2009) HSP70 confers protection against indomethacin-induced lesions of the small intestine. J Pharmacol Exp Ther 330: 458-467. doi:10.1124/jpet.109.152181. PubMed: 19458285.
17. Suemasu S, Tanaka K, Namba T, Ishihara T, Katsu T et al. (2009) A role for HSP70 in protecting against indomethacin-induced gastric lesions. J Biol Chem 284: 19705-19715. doi:10.1074/jbc.M109.006817. PubMed: 19439408.
18. Tanaka K, Ishihara T, Azuma A, Kudoh S, Ebina M et al. (2010) Therapeutic effect of lecithinized superoxide dismutase on bleomycin-induced pulmonary fibrosis. Am J Physiol Lung Cell Mol Physiol 298: L348-L360. doi:10.1152/ajplung.00289.2009. PubMed: 20034962.
19. Hoshino T, Matsuda M, Yamashita Y, Takehara M, Fukuya M et al. (2010) Suppression of melanin production by expression of HSP70. J Biol Chem 285: 13254-13263. doi:10.1074/jbc.M110.103051. PubMed: 20177067.
20. Matsuda M, Hoshino T, Yamashita Y, Tanaka K, Maji D et al. (2010) Prevention of UVB radiation-induced epidermal damage by expression of heat shock protein 70. J Biol Chem 285: 5848-5858. doi:10.1074/jbc.M109.063453. PubMed: 20018843.
21. Evans CG, Wisén S, Gestwicki JE (2006) Heat shock proteins 70 and 90 inhibit early stages of amyloid beta-(1-42) aggregation in vitro. J Biol Chem 281: 33182-33191. doi:10.1074/jbc.M606192200. PubMed: 16973602.
22. Muchowski PJ, Wacker JL (2005) Modulation of neurodegeneration by molecular chaperones. Nat Rev Neurosci 6: 11-22. doi:10.1038/nrn1587. PubMed: 15611723.
23. Calderwood SK, Mambula SS, Gray PJ Jr., Theriault JR (2007) Extracellular heat shock proteins in cell signaling. FEBS Lett 581: 3689-3694. doi:10.1016/j.febslet.2007.04.044. PubMed: 17499247.
24. Magrané J, Smith RC, Walsh K, Querfurth HW (2004) Heat shock protein 70 participates in the neuroprotective response to intracellularly expressed beta-amyloid in neurons. J Neurosci 24: 1700-1706. doi: 10.1523/JNEUROSCI.4330-03.2004. PubMed: 14973234.
25. Kumar P, Ambasta RK, Veereshwarayya V, Rosen KM, Kosik KS et al. (2007) CHIP and HSPs interact with beta-APP in a proteasome-dependent manner and influence Abeta metabolism. Hum Mol Genet 16: 848-864. doi:10.1093/hmg/ddm030. PubMed: 17317785.
26. Kakimura J, Kitamura Y, Takata K, Umeki M, Suzuki S et al. (2002) Microglial activation and amyloid-beta clearance induced by exogenous heat-shock proteins. FASEB J 16: 601-603. PubMed: 11919167.
27. Hoshino T, Murao N, Namba T, Takehara M, Adachi H et al. (2011) Suppression of Alzheimer's disease-related phenotypes by expression of heat shock protein 70 in mice. J Neurosci 31: 5225-5234. doi: 10.1523/JNEUROSCI.5478-10.2011. PubMed: 21471357.

28. Hirakawa T, Rokutan K, Nikawa T, Kishi K (1996) Geranylgeranylacetone induces heat shock proteins in cultured guinea pig gastric mucosal cells and rat gastric mucosa. Gastroenterology 111: 345-357. doi:10.1053/gast.1996.v111.pm8690199. PubMed: 8690199
29. Tanaka K, Tanaka Y, Namba T, Azuma A, Mizushima T (2010) Heat shock protein 70 protects against bleomycin-induced pulmonary fibrosis in mice. Biochem Pharmacol 80: 920-931. doi:10.1016/j.bcp.2010.05.025. PubMed: 20513440.
30. Sturchler-Pierrat C, Abramowski D, Duke M, Wiederhold KH, Mistl C et al. (1997) Two amyloid precursor protein transgenic mouse models with Alzheimer disease-like pathology. Proc Natl Acad Sci U S A 94: 13287-13292. doi:10.1073/pnas.94.24.13287. PubMed: 9371838.
31. Sumigama K, Nakao K, Iwama T, Wakabayashi T, Ohgoh T et al. (1983) Acute toxicity test of tetraprenylacetone in rats and mice. Prog Med 3: 1053-1057.
32. Laurén J, Gimbel DA, Nygaard HB, Gilbert JW, Strittmatter SM (2009) Cellular prion protein mediates impairment of synaptic plasticity by amyloid-beta oligomers. Nature 457: 1128-1132. doi:10.1038/nature07761. PubMed: 19242475.
33. Piermartiri TC, Figueiredo CP, Rial D, Duarte FS, Bezerra SC et al. (2010) Atorvastatin prevents hippocampal cell death, neuroinflammation and oxidative stress following amyloid-beta(1-40) administration in mice: evidence for dissociation between cognitive deficits and neuronal damage. Exp Neurol 226: 274-284. doi:10.1016/j.expneurol.2010.08.030. PubMed: 20816828.
34. Kim DH, Jung WY, Park SJ, Kim JM, Lee S et al. (2010) Anti-amnesic effect of ESP-102 on Abeta(1-42)-induced memory impairment in mice. Pharmacol Biochem Behav 97: 239-248. doi:10.1016/j.pbb.2010.08.005. PubMed: 20728465.
35. Iwata N, Mizukami H, Shirotani K, Takaki Y, Muramatsu S et al. (2004) Presynaptic localization of neprilysin contributes to efficient clearance of amyloid-beta peptide in mouse brain. J Neurosci 24: 991-998. doi: 10.1523/JNEUROSCI.4792-03.2004. PubMed: 14749444.
36. Katsuno M, Sang C, Adachi H, Minamiyama M, Waza M et al. (2005) Pharmacological induction of heat-shock proteins alleviates polyglutamine-mediated motor neuron disease. Proc Natl Acad Sci U S A 102: 16801-16806. doi:10.1073/pnas.0506249102. PubMed: 16260738.
37. Rijal Upadhaya A, Capetillo-Zarate E, Kosterin I, Abramowski D, Kumar S et al. (2012) Dispersible amyloid beta-protein oligomers, protofibrils, and fibrils represent diffusible but not soluble aggregates: their role in neurodegeneration in amyloid precursor protein (APP) transgenic mice. Neurobiol Aging 33: 2641-2660. doi:10.1016/j.neurobiolaging.2011.12.032. PubMed: 22305478.
38. Adachi H, Katsuno M, Minamiyama M, Sang C, Pagoulatos G et al. (2003) Heat shock protein 70 chaperone overexpression ameliorates phenotypes of the spinal and bulbar muscular atrophy transgenic mouse model by reducing nuclear-localized mutant androgen receptor protein. J Neurosci 23: 2203-2211. PubMed: 12657679.
39. Nishizawa Y, Tanaka H, Kinoshita K (1983) Administration, distribution, metabolism and excretion of tetraprenylacetone in rats and guinea pig. Prog Med 3: 1029-1035.
40. Seno K, Joh T, Yokoyama Y, Itoh M (1995) Role of mucus in gastric mucosal injury induced by local ischemia/reperfusion. J Lab Clin Med 126: 287-293. PubMed: 7665977.
41. Yasuda H, Shichinohe H, Kuroda S, Ishikawa T, Iwasaki Y (2005) Neuroprotective effect of a heat shock protein inducer, geranylgeranylacetone in permanent focal cerebral ischemia. Brain Res 1032: 176-182. doi:10.1016/j.brainres.2004.11.009. PubMed: 15680957.
42. Sinn DI, Chu K, Lee ST, Song EC, Jung KH et al. (2007) Pharmacological induction of heat shock protein exerts neuroprotective effects in experimental intracerebral hemorrhage. Brain Res 1135: 167-176. doi:10.1016/j.brainres.2006.11.098. PubMed: 17208204.
43. Labbadia J, Cunliffe H, Weiss A, Katsyuba E, Sathasivam K et al. (2011) Altered chromatin architecture underlies progressive impairment of the heat shock response in mouse models of Huntington disease. J Clin Invest 121: 3306-3319. doi:10.1172/JCI57413. PubMed: 21785217.
44. Abe E, Fujiki M, Nagai Y, Shiqi K, Kubo T et al. (2010) The phosphatidylinositol-3 kinase/Akt pathway mediates geranylgeranylacetone-induced neuroprotection against cerebral infarction in rats. Brain Res 1330: 151-157. doi:10.1016/j.brainres.2010.02.074. PubMed: 20206146.
45. Tanito M, Kwon YW, Kondo N, Bai J, Masutani H et al. (2005) Cytoprotective effects of geranylgeranylacetone against retinal photooxidative damage. J Neurosci 25: 2396-2404. doi:10.1523/JNEUROSCI.4866-04.2005. PubMed: 15745966.
46. Kunisaki C, Sugiyama M (1992) Effect of teprenone on acute gastric mucosal lesions induced by cold-restraint stress. Digestion 53: 45-53. doi:10.1159/000200970. PubMed: 1289172.
47. Oketani K, Murakami M, Fujisaki H, Wakabayashi T, Hotta K (1983) Effect of geranylgeranylacetone on aspirin-induced changes in gastric glycoproteins. Jpn J Pharmacol 33: 593-601. doi:10.1254/jjp.33.593. PubMed: 6620729.
48. Ushijima H, Tanaka K, Takeda M, Katsu T, Mima S et al. (2005) Geranylgeranylacetone protects membranes against nonsteroidal anti-inflammatory drugs. Mol Pharmacol 68: 1156-1161. doi:10.1124/mol.105.015784. PubMed: 16046660.
49. Ikeda M, Kawai Y, Mori K, Yano M, Abe K et al. (2011) Anti-ulcer agent teprenone inhibits hepatitis C virus replication: potential treatment for hepatitis C. Liver Int 31: 871-880. doi:10.1111/j.1478-3231.2011.02499.x. PubMed: 21645219.
50. Takeshita S, Ichikawa T, Taura N, Miyaaki H, Matsuzaki T et al. (2012) Geranylgeranylacetone has anti-hepatitis C virus activity via activation of mTOR in human hepatoma cells. J Gastroenterol 47: 195-202. doi: 10.1007/s00535-011-0481-z. PubMed: 22038554.

nature COMMUNICATIONS

ARTICLE

Received 20 Aug 2013 Accepted 30 Sep 2013 Published 5 Nov 2013

DOI: 10.1038/ncomms3686

Mepenzolate bromide displays beneficial effects in a mouse model of chronic obstructive pulmonary disease

Ken-Ichiro Tanaka[1], Tomoaki Ishihara[1], Toshifumi Sugizaki[1], Daisuke Kobayashi[1], Yasunobu Yamashita[1], Kayoko Tahara[1], Naoki Yamakawa[1], Kumiko Iijima[2], Kaoru Mogushi[2], Hiroshi Tanaka[2], Keizo Sato[3], Hidekazu Suzuki[4] & Tohru Mizushima[1]

The clinical treatment of chronic obstructive pulmonary disease (COPD) requires not only an improvement of airflow by bronchodilation but also the suppression of emphysema by controlling inflammation. Here we screen a compound library consisting of clinically used drugs for their ability to prevent elastase-induced airspace enlargement in mice. We show that intratracheal administration or inhalation of mepenzolate bromide, a muscarinic antagonist used to treat gastrointestinal disorders, decreases the severity of elastase-induced airspace enlargement and respiratory dysfunction. Although mepenzolate bromide shows bronchodilatory activity, most other muscarinic antagonists do not improve elastase-induced pulmonary disorders. Apart from suppressing elastase-induced pulmonary inflammatory responses and the production of superoxide anions, mepenzolate bromide reduces the level of cigarette smoke-induced airspace enlargement and respiratory dysfunction. Based on these results, we propose that mepenzolate bromide may be an effective therapeutic for the treatment of COPD due to its anti-inflammatory and bronchodilatory activities.

[1] Department of Analytical Chemistry, Faculty of Pharmacy, Keio University, 1-5-30, Shibakoen, Minato-ku, Tokyo 105 8512, Japan. [2] Division of Medical Genomics, Department of Bioinformatics, Medical Research Institute, Tokyo Medical and Dental University, 1-5-45, Yushima, Bunkyo-ku, Tokyo 113 8510, Japan. [3] Kyushu University of Health and Welfare, 1714-1, Yoshino-cho, Nobeoka 882 8508, Japan. [4] Division of Gastroenterology and Hepatology, Department of Internal Medicine, Keio University School of Medicine, 35, Shinanomachi, Shinjuku-ku, Tokyo 160 8582, Japan. Correspondence and requests for materials should be addressed to T.M. (email: mizushima-th@pha.keio.ac.jp).

Chronic obstructive pulmonary disease (COPD) is a serious health problem whose most important etiologic factor is cigarette smoke (CS)[1]. COPD is a disease that is defined by a progressive and partially reversible airflow limitation associated with abnormal inflammatory responses and permanent enlargement of the pulmonary airspace[1–3]. Thus, for the clinical treatment of COPD, it is important not only to improve the airflow limitation by bronchodilation, but also to suppress disease progression by controlling inflammatory processes.

Bronchodilators (β_2-agonists and muscarinic antagonists) are currently used for the treatment of COPD, providing an effective temporary improvement of airflow limitation[2,4,5]. On the other hand, steroids are used to suppress the inflammatory responses associated with COPD. However, steroids cannot significantly modulate disease progression and mortality[5,6] because the inflammation associated with COPD shows resistance to steroid treatment[7].

In addition to the fact that CS contains a high concentration of reactive oxygen species (ROS), activated leukocytes also produce large amounts of ROS, with one such example being the superoxide anions produced *via* the activation of nicotinamide adenine dinucleotide phosphate (NADPH) oxidase[8]. In contrast to this, the body contains a number of endogenous antioxidant proteins such as superoxide dismutase (SOD) and glutathione *S*-transferase (GST), with a decrease in these proteins reported to be involved in the pathogenesis of COPD[9,10]. The inflammatory responses associated with COPD are thought to be triggered by oxidative stress and mediated through the activation of nuclear factor-κB (NF-κB, a pro-inflammatory transcription factor) and inhibition of histone deacetylase 2 (HDAC2)[11–14]. Oxidative stress seems to activate NF-κB through the inhibition of HDAC activity and degradation of inhibitor of NF-κB (IκB)-α (refs 12,14,15). Pro-inflammatory gene expression is normally silenced by the condensation of DNA; however, the acetylation of core histones opens up the condensed chromatin and induces the expression of these genes (refs 11,12,16). HDACs suppress the expression of pro-inflammatory genes not only by maintaining chromatin condensation but also by directly modifying pro-inflammatory transcription factors (such as NF-κB)[12]. Moreover, HDACs, and particularly HDAC2, seem to have important roles in the inflammatory responses associated with COPD[11,17,18]. Furthermore, because corticosteroids use HDAC2 to suppress the activity of NF-κB[11,12,19], the inhibitory effect of CS on HDAC2 may be responsible for the reduced sensitivity of COPD patients to steroid treatment[11]. Therefore, compounds that activate HDAC2 or inhibit ROS production and NF-κB may be effective for the treatment of inflammation associated with COPD.

In the present study, we screen compounds that prevent elastase-induced airspace enlargement in mice from a library of existing medicines whose safety properties have already been well characterized in humans. We select mepenzolate bromide (mepenzolate), which is an orally administered muscarinic receptor antagonist used to treat gastrointestinal disorders[20–22], and administer this compound to mice, which suppresses elastase-induced pulmonary inflammatory responses, airspace enlargement, alteration of lung mechanics and respiratory dysfunction. We also found that mepenzolate has bronchodilatory activity. These results suggest that mepenzolate achieves its anti-inflammatory effect *via* muscarinic receptor-independent inhibitory effects on NF-κB and NADPH oxidase, together with stimulatory effects on HDAC2, SOD and GST. We suggest that mepenzolate could provide an effective treatment option for COPD, not only as a consequence of its bronchodilatory activity but also due to its anti-inflammatory properties.

Results

Effect of mepenzolate on airspace enlargement. From a group of 83 medicines already in clinical use (Supplementary Table S1), we screened for compounds able to suppress porcine pancreatic elastase (PPE)-induced airspace enlargement. Each drug was administered intraperitoneally to mice, and after selecting eight candidate compounds based on the level of suppression of airspace enlargement (Supplementary Table S1), these were administered intratracheally at various doses and their inhibitory effects on PPE-induced airspace enlargement evaluated. Following this process, mepenzolate was selected based on the level of suppression of airspace enlargement it provided at clinical dose or less.

Histopathological analysis of pulmonary tissue using hematoxylin and eosin (H&E) staining revealed that PPE administration induced airspace enlargement (increase in the mean linear intercept (MLI)) and that the simultaneous daily intratracheal administration of mepenzolate suppressed this enlargement in a dose-dependent manner (Fig. 1a,b).

The alteration of lung mechanics associated with pulmonary emphysema is characterized by a decrease in elastance. Total respiratory system elastance (elastance of the whole lung, including the bronchi, bronchioles and alveoli) and tissue elastance (elastance of alveoli) were decreased by the PPE treatment in a manner that could be restored in part by the simultaneous administration of mepenzolate, again in a dose-dependent manner (Fig. 1c).

We next examined the effect of mepenzolate administered by the inhalation route on the PPE-induced airspace enlargement and alteration of lung mechanics. The results obtained (Fig. 1d–f) were similar to those observed with the intratracheal mode of administration (Fig. 1a–c).

To determine the effect of mepenzolate on pre-developed pulmonary emphysema, the intratracheal administration of mepenzolate to mice was commenced 14 days after the administration of PPE, and airspace enlargement and lung mechanics were assessed on day 21. Compared with vehicle-treated animals, mepenzolate decreased the extent of PPE-induced airspace enlargement and alterations to lung mechanics (Fig. 2a–c), suggesting that mepenzolate could be an effective compound for the treatment of pre-developed pulmonary emphysema.

Effects of other muscarinic antagonists. We next examined the effects of other muscarinic antagonists on PPE-induced airspace enlargement and alterations of lung mechanics. Even at the highest dose, none of muscarinic antagonists tested significantly suppressed the PPE-induced airspace enlargement or alterations in lung mechanics (Fig. 3a–c).

The diagnosis of COPD is confirmed by a decrease in the ratio of forced expiratory volume in the first second (FEV_1) to forced vital capacity (FVC)[1]. We recently established a technique to monitor PPE-induced respiratory dysfunction in mice, and found that the $FEV_{0.05}$/FVC ratio clearly decreased in PPE-treated mice compared with control mice[23]. Using this technique, we examined here the effects of mepenzolate and other muscarinic antagonists on the PPE-induced decrease in $FEV_{0.05}$/FVC. To washout the bronchodilatory effect of the muscarinic antagonists, the administration of each drug was discontinued on day 10 and the assay performed on day 14. PPE treatment decreased the $FEV_{0.05}$/FVC ratio, whereas the simultaneous administration of mepenzolate, but not the other muscarinic antagonists, restored the $FEV_{0.05}$/FVC towards control values (Fig. 3d). The results in Fig. 3 show that ipratropium bromide (ipratropium), scopolamine *N*-butylbromide (scopolamine) and pirenzepine

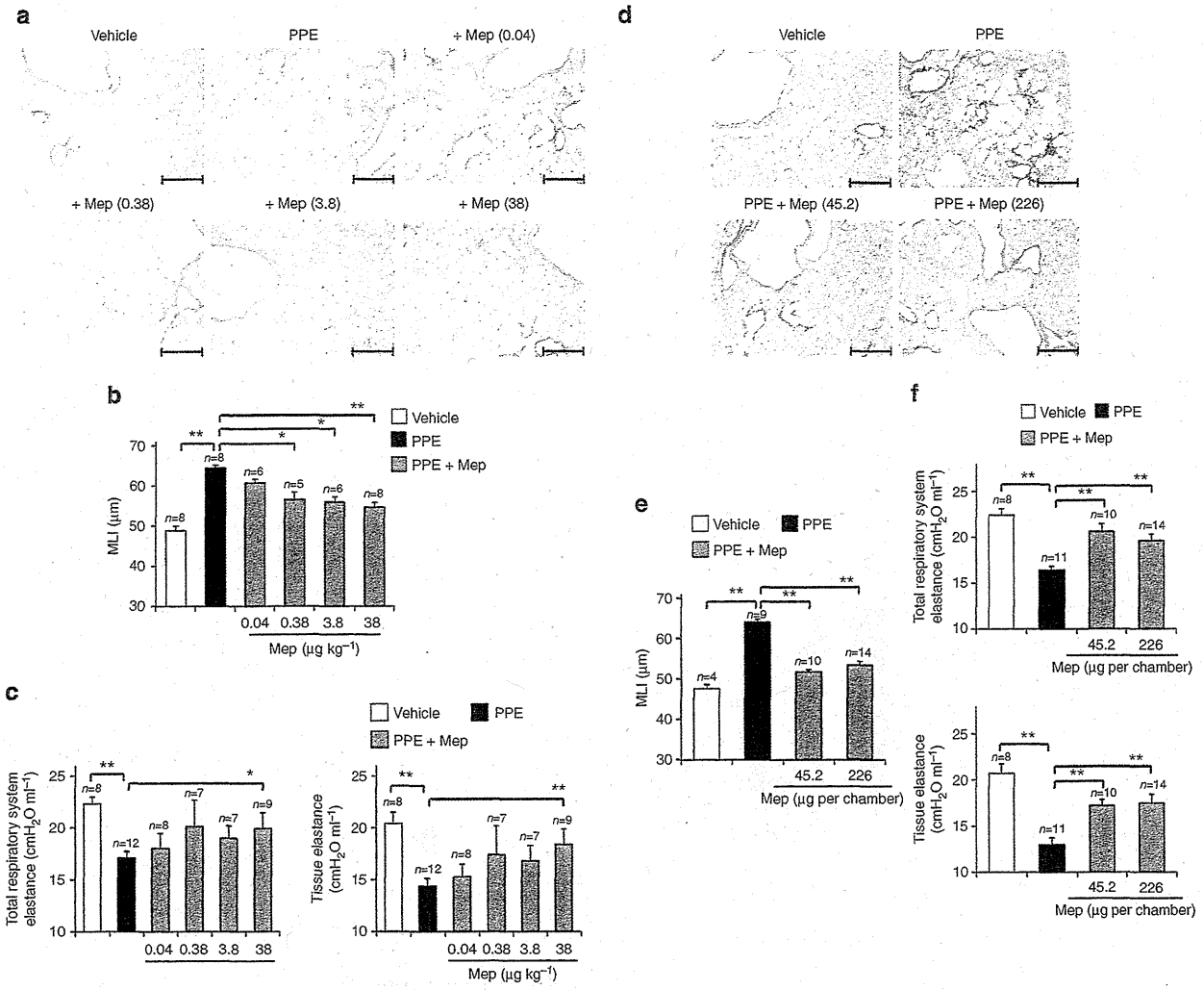

Figure 1 | Effect of mepenzolate on PPE-induced pulmonary disorders. Mice were treated with PPE (100 μg per mouse) once only on day 0 or with the vehicle only. The indicated doses (**a–c**, μg kg^{-1}; **d–f**, μg per chamber) of mepenzolate (Mep) were administered intratracheally (**a–c**) or by inhalation (**d–f**) once daily for 14 days (from day 0 to day 13). Sections of pulmonary tissue were prepared on day 14 and subjected to histopathological examination (H&E staining) (scale bar, 500 μm) (**a**,**d**). Airspace size was estimated by determining the MLI as described in the Materials and Methods (**b**,**e**). Total respiratory system elastance and tissue elastance were determined on day 14 as described in the Methods (**c**,**f**). Values represent the mean ± s.e.m. *$P<0.05$; **$P<0.01$ (Tukey test). Experiments were replicated at least two times.

dihydrochloride (pirenzepine) were not effective in combatting PPE-induced airspace enlargement, nor did they improve lung mechanics or respiratory dysfunction. This finding suggests that mepenzolate achieves its ameliorative effect over PPE-induced pulmonary disorders *via* mechanisms that are independent of its effects on muscarinic receptors and bronchodilatory activity.

To further test this idea, we examined the bronchodilatory activity induced by the muscarinic antagonists mentioned above. As shown in Fig. 4a, the dose-dependent increase in airway resistance (bronchoconstriction) induced by inhaled methacholine was completely suppressed by the intratracheal pre-administration of mepenzolate, thus attesting to the latter's bronchodilatory activity. The dose-response profile of ipratropium for bronchodilation was similar to that of mepenzolate (Fig. 4a), although ipratropium had no effect against the PPE-induced pulmonary disorders (Fig. 3). Neither scopolamine nor pirenzepine showed bronchodilatory activity, at least not at the highest dose employed here (Supplementary Fig. S1). These results further support the notion that mepenzolate achieves its ameliorative effect against PPE-induced pulmonary disorders *via* muscarinic receptor- and bronchodilatory activity-independent mechanisms. In addition, the results in Fig. 4b show that, as for ipratropium, the bronchodilatory activity of mepenzolate was transient, diminishing 48 h after its administration.

Muscarinic antagonists used to treat COPD are categorized as being long acting (such as tiotropium bromide (tiotropium) and glycopyrronium bromide (glycopyrronium)) or short acting (such as ipratropium), with the long-acting muscarinic antagonists now considered the standard bronchodilator treatment for COPD[24]. We subsequently examined the effect of intratracheal administration of tiotropium or glycopyrronium on PPE-induced pulmonary disorders. As shown in Supplementary Fig. S2a–c, glycopyrronium suppressed the PPE-induced airspace enlargement and alterations of lung mechanics. However, the extent of amelioration of airspace enlargement was not as apparent as that seen with mepenzolate (Supplementary Fig. S2b), and glycopyrronium did not significantly suppress the PPE-induced respiratory dysfunction (Supplementary Fig. S2d).

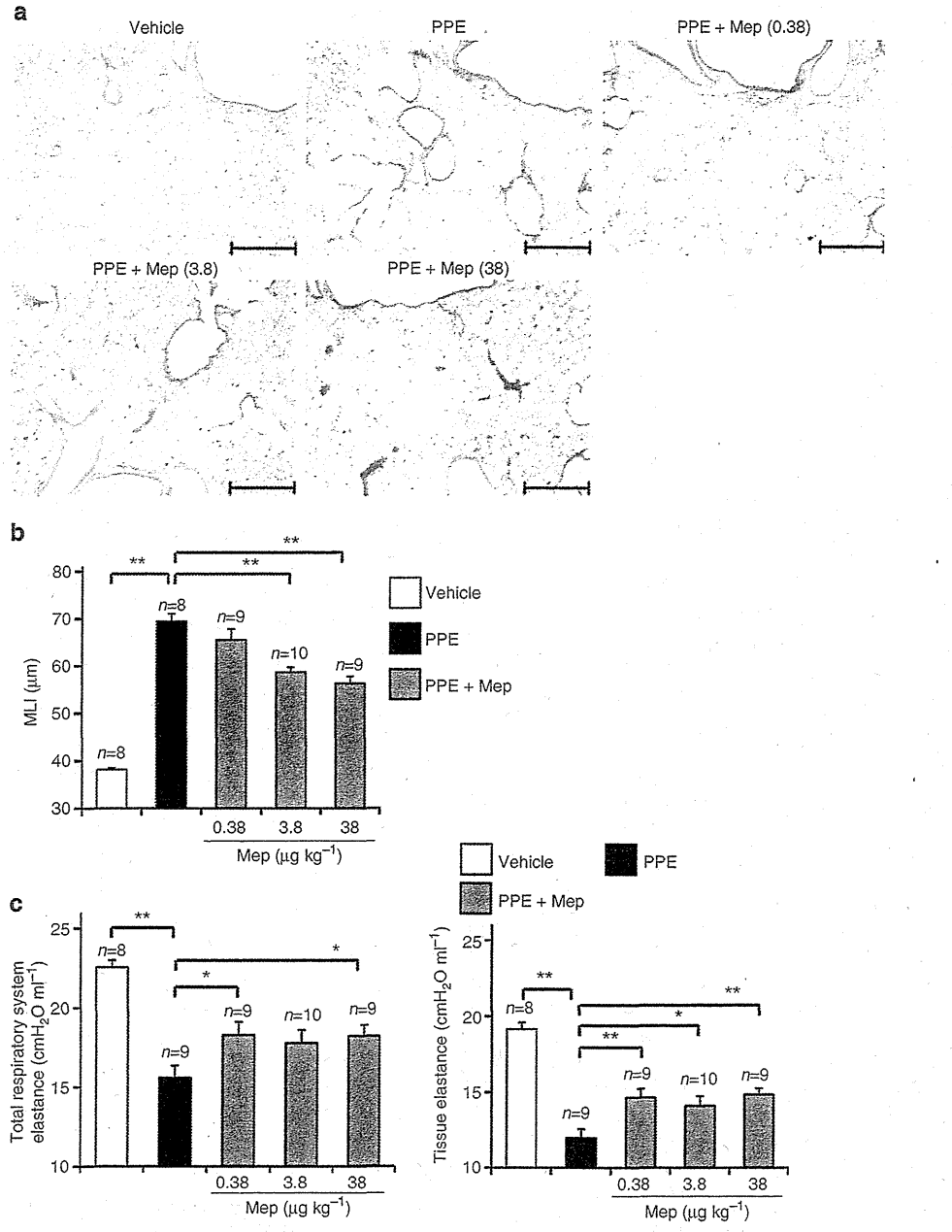

Figure 2 | Effect of mepenzolate on pre-developed pulmonary emphysema. Mice were treated with PPE (100 μg per mouse) once only on day 0 or with the vehicle only. The indicated doses ($\mu g\,kg^{-1}$) of mepenzolate (Mep) were administered intratracheally once daily from day 14 to day 20. Sections of pulmonary tissue were prepared on day 21 and subjected to histopathological examination (H&E staining) (scale bar, 500 μm) (**a**). Airspace size was estimated by determining the MLI as described in the Materials and Methods (**b**). Total respiratory system elastance and tissue elastance were determined on day 21 as described in the Methods (**c**). Values represent the mean ± s.e.m. *$P<0.05$; **$P<0.01$ (Tukey test). Experiments were replicated at least two times.

On the other hand, tiotropium did not suppress the PPE-induced airspace enlargement, alterations of lung mechanics or respiratory dysfunction (except for a weak suppression of tissue elastance at the $30\,\mu g\,kg^{-1}$ dose) (Supplementary Fig. S2a–d).

Effect of mepenzolate on inflammatory responses. We next monitored PPE-induced pulmonary inflammatory responses by determining the number of leucocytes in bronchoalveolar lavage fluid (BALF) 24 h after the administration of PPE. As shown in Fig. 5a, the total number of leucocytes and individual number of neutrophils were increased by the PPE treatment and this effect was suppressed by the simultaneous administration of mepenzolate. We also examined the levels of pro-inflammatory cytokines (tumour necrosis factor-α) and chemokines (macrophage inflammatory protein-2, monocyte chemoattractant protein-1 and keratinocyte-derived chemokine) in BALF. Levels of these pro-inflammatory cytokines and chemokines increased after the PPE treatment, and this increase was suppressed by the simultaneous treatment of animals with mepenzolate (Fig. 5b). These

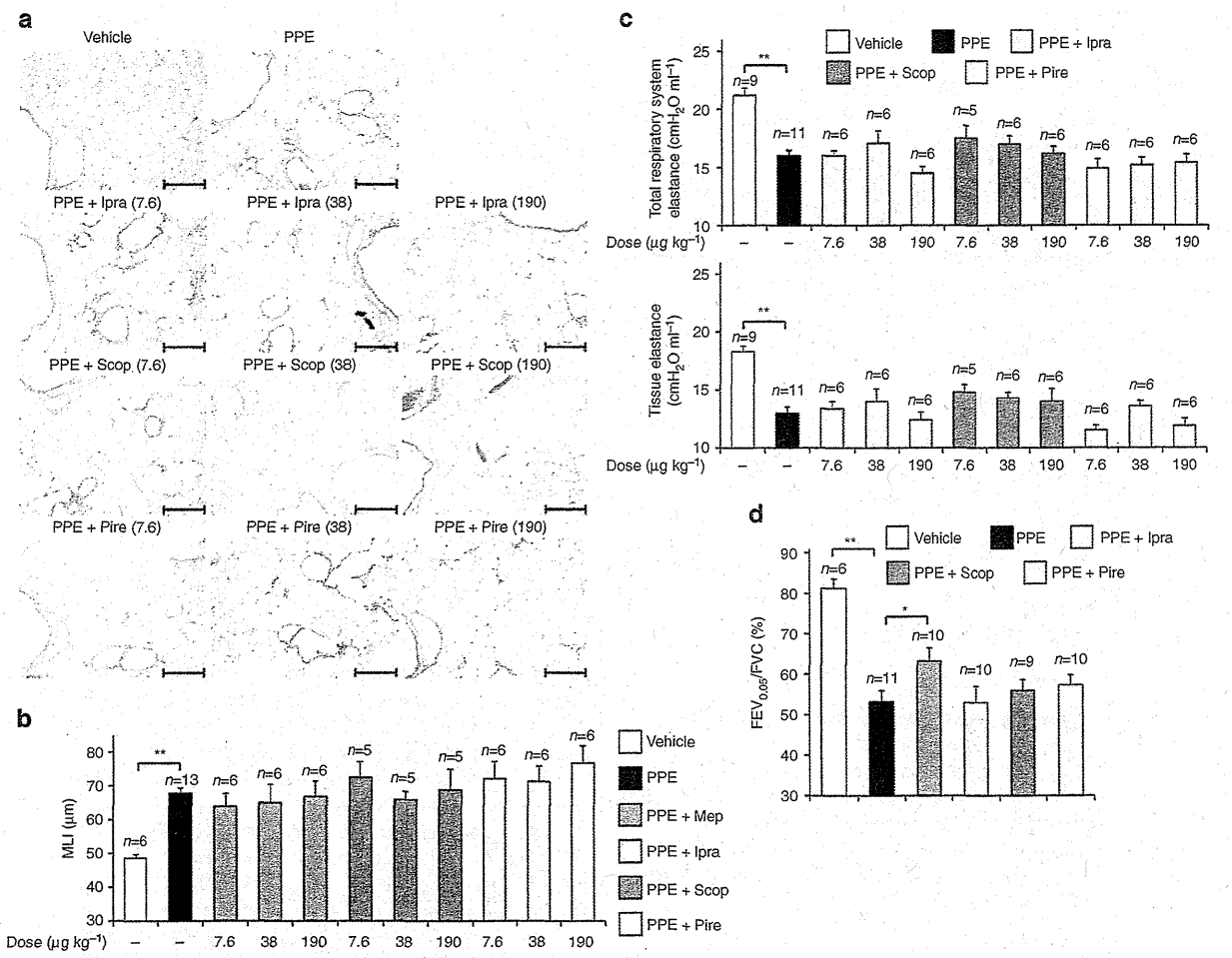

Figure 3 | Effect of different muscarinic antagonists on PPE-induced pulmonary disorders. Mice were treated with PPE (100 μg per mouse) once only on day 0 or with the vehicle only. The indicated doses (μg kg^{-1}) (**a–c**) or 38 μg kg^{-1} (**d**) of ipratropium (Ipra) (**a–d**), scopolamine (Scop) (**a–d**), pirenzepine (Pire) (**a–d**) or mepenzolate (Mep) (**d**) were administered intratracheally once daily for 14 days (from day 0 to day 13) (**a–c**) or for 11 days (from day 0 to day 10) (**d**). Sections of pulmonary tissue were prepared on day 14 and subjected to histopathological examination (H&E staining) (scale bar, 500 μm) (a). Airspace size was estimated by determining the MLI as described in the Materials and Methods (**b**). Total respiratory system elastance and tissue elastance were determined on day 14 as described in the Methods (**c**). The $FEV_{0.05}$/FVC was determined on day 14 as described in the Materials and Methods (**d**). Values represent the mean ± s.e.m. *$P<0.05$; **$P<0.01$ (Tukey test). Experiments were replicated at least two times.

results suggest that mepenzolate could achieve its ameliorative effect by suppressing PPE-induced inflammatory responses.

We then focused on NF-κB and its regulator, HDAC2. The level of the Ser536-phosphorylated (active) form of NF-κB detected by immunohistochemical analysis increased in response to the PPE treatment, and could be suppressed by the simultaneous treatment of animals with mepenzolate (Fig. 5c). The level of IκB-α was decreased by the PPE treatment and remained stable when mepenzolate was concomitantly administered (Fig. 5d,e).

As shown in Fig. 5f, *Hdac2* mRNA expression was suppressed by the PPE treatment and could be partially restored by the simultaneous treatment of animals with mepenzolate. This alteration was also observed at the protein level (Fig. 5d,e). Furthermore, the enzymatic activity of HDAC was also decreased by the PPE treatment and could be partially restored by the simultaneous administration of mepenzolate (Fig. 5g). These results suggest that mepenzolate achieves its anti-inflammatory activity by increasing or decreasing the activity of HDAC2 or NF-κB, respectively.

Effect of mepenzolate on superoxide anion production. Electron spin resonance (ESR) analysis was employed to examine the effect of mepenzolate on the production of superoxide anions in mice. As shown in Fig. 6a,b, the peak amplitude corresponding to the superoxide anion level was higher in cells prepared from PPE-administered mice than in those from control mice. The peak amplitude in cells prepared from mice administered both PPE and mepenzolate was lower than that of mice administered PPE only (Fig. 6a,b), suggesting that mepenzolate suppresses the PPE-induced production of superoxide anions in the lung. The NADPH oxidase activity of cells in BALF was increased by the PPE treatment and could be partially suppressed by the simultaneous treatment of animals with mepenzolate (Fig. 6c). This suppression was observed at 4, 8 and 24 h but not 1 h after the administration of mepenzolate (Fig. 6c), suggesting that mepenzolate is a modulator of NADPH activation, but not an enzyme inhibitor of NADPH oxidase. On the other hand, the mRNA and protein expression of SOD1 and the enzymatic activity of SOD in the lung were decreased by the PPE treatment, with these effects also suppressed by the simultaneous

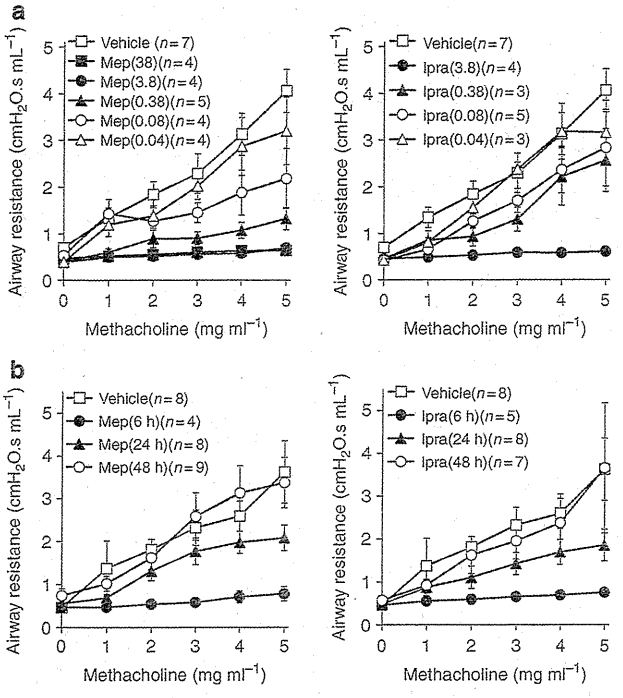

Figure 4 | Effect of mepenzolate on methacholine-induced airway constriction. Indicated doses (μg kg^{-1}) (**a**) or 38 μg kg^{-1} (**b**) of mepenzolate (Mep) or ipratropium (Ipra) were administered intratracheally. After 1 h (**a**) or indicated period (**b**), mice were exposed to nebulized methacholine five times and airway resistance was determined after each methacholine challenge as described in the Materials and Methods. Values are mean ± s.e.m. Experiments were replicated at least two times.

administration of mepenzolate (Fig. 5d–g). These results suggest that mepenzolate suppresses the PPE-induced increase in superoxide anion production by modulating the activation of NADPH oxidase or activating SOD1.

We subsequently tested whether mepenzolate directly affects superoxide anion production *in vitro*. Cells prepared from the BALF of PPE-treated mice were incubated with a spin trap agent in the presence or absence of mepenzolate. As shown in Fig. 6d,e, mepenzolate decreased the level of superoxide anions in a dose-dependent manner, the extent of which was similar to that seen with apocynin (an inhibitor of NADPH oxidase). We found that the intratracheal administration of apocynin partially suppressed PPE-induced airspace enlargement and alterations of lung mechanics (Supplementary Fig. S3). These findings suggest that most of the superoxide anions were produced by NADPH oxidase under these conditions and that mepenzolate could modulate NADPH oxidase activity and thus reduce the production of superoxide anions and PPE-induced pulmonary disorders.

To understand the mechanism of the inhibitory effect of mepenzolate on NADPH oxidase activity, we examined the effect of mepenzolate on the PPE-dependent alteration of mRNA expression of genes related to NADPH oxidase (such as *p91^{phox}(Nox2)*, *p22^{phox}*, *p40^{phox}*, *p47^{phox}*, *p67^{phox}* and *Rac2*). As shown in Supplementary Fig. S4a, PPE treatment upregulated the mRNA expression of these genes in a manner that could be suppressed by concomitant administration of mepenzolate. The mRNA expression of some of other *Noxs* (*Nox1, 4*) and dual oxidases (*Duoxs*; *Duox1, 2*) was also affected by treatment with PPE and/or mepenzolate (Supplementary Fig. S4b). Furthermore, treatment of cells in BALF with phorbol 12-myristate 13-acetate (PMA) activated NADPH oxidase, whereas pretreatment of cells with mepenzolate decreased this activity in the presence of PMA treatment but not in its absence (Fig. 6f). This finding supports the notion that mepenzolate is a modulator of NADPH activation, but not an enzyme inhibitor of NADPH oxidase. Taken together, these results suggest that the modulatory effect of mepenzolate on NADPH oxidase activity can be explained in terms of its downmodulation of the expression of NADPH oxidase-related genes and the activation of this enzyme.

To further understand the mechanism governing the mepenzolate-dependent decrease in inflammatory responses and oxidative stress, we performed DNA microarray analysis of lung tissue from mepenzolate-treated (or control) mice. Among the genes whose expression was altered by the mepenzolate administration (Table 1), we focused on genes encoding GSTs that were included in a 'glutathione metabolism' gene set (Supplementary Fig. S5a,b) and are known to reduce oxidative stress by decreasing lipid peroxide levels[9]. As shown in Fig. 7a,b, the mRNA expression of *Gst* genes and GST activity in the lung were increased by the mepenzolate administration. The mepenzolate administration also restored GST activity, which was decreased by the PPE treatment (Fig. 7c). It was reported that GST and its regulatory transcription factor, NF-E2-related factor 2 (Nrf2), in macrophages have an important role in the pathogenesis of COPD[25,26]. Therefore, we performed the Gene Set Enrichment Analysis using the custom gene set and confirmed that the downstream genes of Nrf2 (NFE2L2 target genes) were upregulated by the mepenzolate administration (Supplementary Fig. S5c,d). Furthermore, we found that treatment of RAW264 cells (a macrophage cell line) with mepenzolate upregulated the mRNA expression *Gst* genes and GST activity (Fig. 7d,e). Mepenzolate also activated Nrf2 and the expression of other Nrf2-regulated genes (heme oxygenase 1 (*Ho1*), NAD(P)H dehydrogenase, quinone1 (*Nqo1*) and *Sod1*) in RAW264 cells (Fig. 7f,g). These results suggest that the stimulatory effect of mepenzolate on Nrf2 activity and the resulting expression of *Gst* genes also involve the mepenzolate-dependent decrease in inflammatory responses and oxidative stress.

Effect of mepenzolate on CS-induced pulmonary disorders. Finally, we examined the effect of the intratracheal administration of mepenzolate on CS-induced pulmonary disorders. As shown in Fig. 8a–c, pulmonary inflammatory responses and airspace enlargement were induced following exposure of mice to CS, with the simultaneous intratracheal administration of mepenzolate clearly suppressing the severity of these CS-induced pulmonary disorders. We also found that the exposure of mice to CS decreased total respiratory system elastance and tissue elastance and that these parameters could be clearly improved by the simultaneous administration of mepenzolate (Fig. 8d). Administration of mepenzolate also suppressed CS-induced increases in oxidative stress (the pulmonary level of 8-hydroxy-2′-deoxyguanosine (8-OHdG)) (Fig. 8e). Mepenzolate increased GST activity in either the presence or absence of CS treatment *in vivo* (Fig. 8f). *In vitro*, GST activity was increased by the treatment of cells with mepenzolate, even in the presence of CS extract (CSE), which itself activated GST (Fig. 8g). On the other hand, we found that mepenzolate suppressed the CS-induced mRNA expression of *Mip-2* and *Kc* and activation of NADPH oxidase (Supplementary Fig. S6a,b). Mepenzolate also restored the HDAC and SOD activities that were decreased by exposure to CS (Supplementary Fig. S6c). These results suggest that mepenzolate protects against CS-induced pulmonary disorders *via* a mechanism similar to that in which it exerts its action against PPE-induced pulmonary disorders.

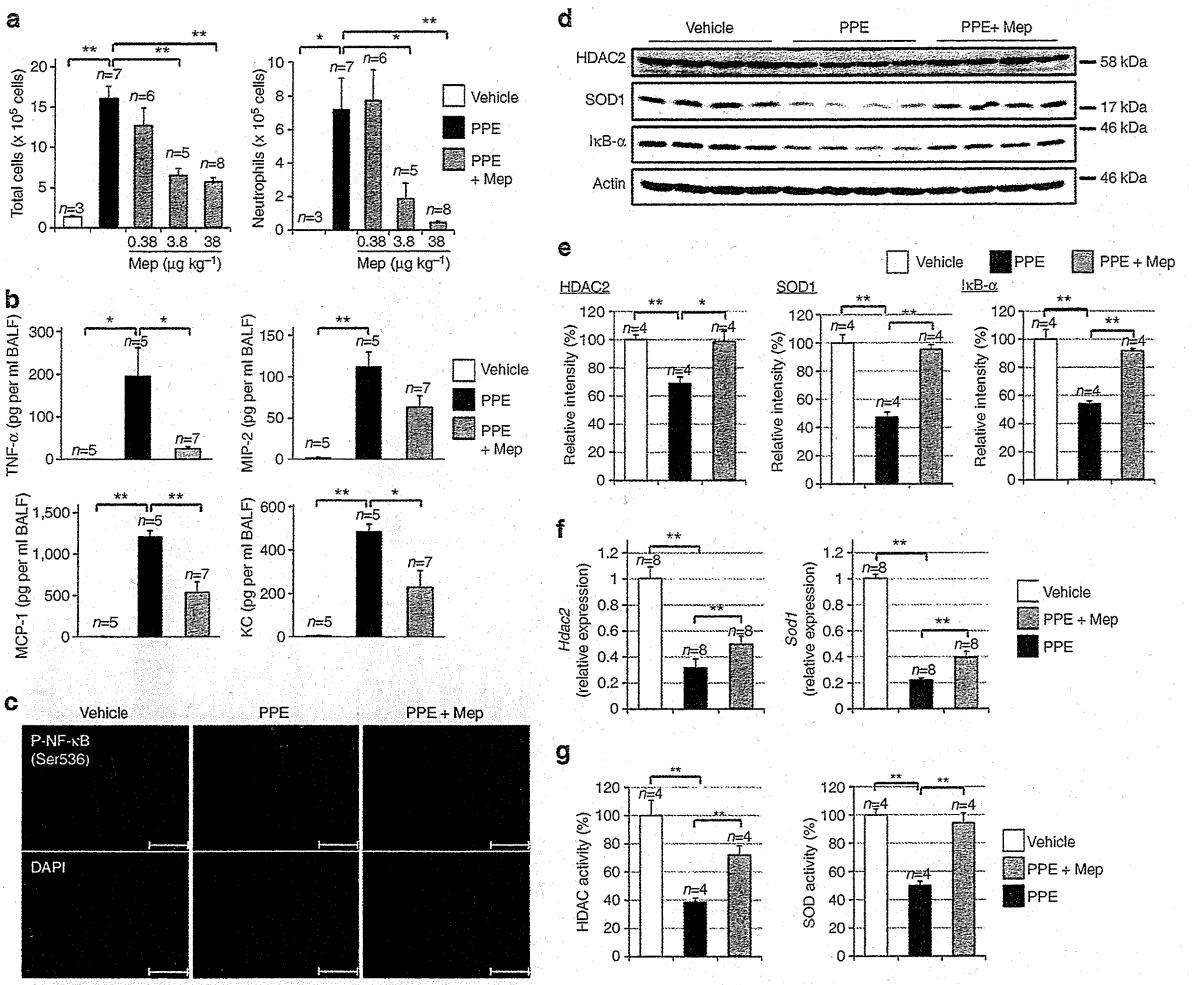

Figure 5 | Effect of mepenzolate on PPE-induced inflammatory responses. Indicated doses (μg kg^{-1}) of mepenzolate (Mep) were administered intratracheally once only. Mice were treated with or without (vehicle) PPE (100 μg per mouse) 1 h after the mepenzolate administration. Twenty-four hours after the PPE administration, BALF (**a**,**b**), sections (**c**) or homogenates (**d**–**g**) were prepared from the lung. The total cell number and the number of neutrophils (**a**) or levels of cytokines and chemokines (**b**) were determined as described in the Materials and Methods. Immunohistochemical analysis with an antibody against the Ser536-phosphorylated form of NF-κB was performed as described in the Materials and Methods (scale bar, 100 μm) (**c**). Samples were analysed by immunoblotting with antibodies against HDAC2, SOD1, IκB-α or actin (**d**). The band intensity of each protein was determined and normalized with respect to actin (**e**). Total RNA was extracted and subjected to real-time RT-PCR using a specific primer set for each gene. Values were normalized to the *Gapdh* gene and expressed relative to the control sample (**f**). The activity of HDAC or SOD was determined as described in the Materials and Methods (**g**). Values represent the mean ± s.e.m. $*P<0.05$; $**P<0.01$ (Tukey test). Experiments were replicated at least two times.

Discussion

The number of drugs reaching the marketplace each year is decreasing, mainly because of the unexpected adverse effects of potential drugs being revealed at advanced stages of clinical trials. To circumvent this, we have proposed a new strategy for drug discovery and development, which focuses on the use of medicines that have already been approved for use by humans (drug repositioning)[27]. In this strategy, compounds with clinically beneficial pharmacological activity are screened from a library of medicines already in clinical use to be developed for new indications. The advantage of this strategy is that there is a decreased risk for unexpected adverse effects in humans because the safety aspects of these drugs have already been well characterized in humans[27]. In the present study, we applied this strategy to screen for drugs to combat COPD. The drug mepenzolate was identified using this approach, and we found that its intratracheal administration suppresses PPE-induced airspace enlargement and alteration of lung mechanics, suggesting that mepenzolate could provide an effective treatment for COPD.

To highlight the potential clinical relevance of our findings, we performed several key experiments. First, we demonstrated that inhalation of mepenzolate was also effective against PPE-induced airspace enlargement and alteration of lung mechanics. This route of administration is noteworthy because of its potential to have less impact on the quality of life of COPD patients given that the drug can be administered on a daily basis at home. Second, we showed that mepenzolate has a therapeutic effect even when the drug was administered after the development of emphysema. We also showed that mepenzolate suppresses the PPE-induced decrease in $FEV_{0.05}$/FVC and finally, we demonstrated that mepenzolate exerts an ameliorative effect against CS-induced pulmonary disorders.

Among the five types of muscarinic receptors ($M_{1-5}R$), M_3R expressed in bronchial smooth muscle can be blocked by

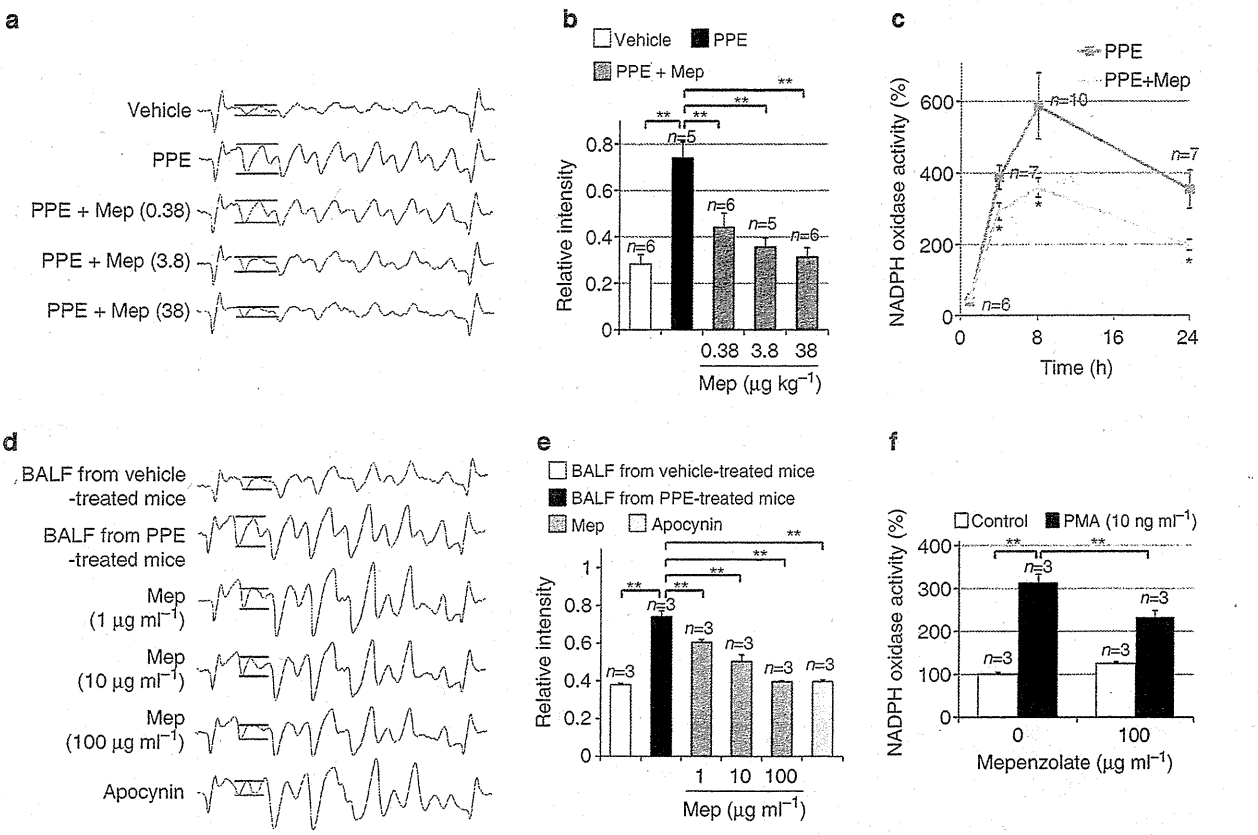

Figure 6 | Effect of mepenzolate on superoxide anion production. (**a**–**c**), indicated doses (μg kg^{-1}) of mepenzolate (Mep) were administered intratracheally once only. Mice were treated with or without (vehicle) PPE (100 μg per mouse) 1 h after the mepenzolate administration. Cells in BALF were prepared 24 h (**a**,**b**) or 1, 4, 8, 24 h (**c**) after the PPE administration. Cells were incubated with a spin trap agent (DPhPMPO) for 10 min and subjected to radical adduct ESR spectrum analysis to determine the amount of superoxide anions present. The intensity of the ESR signal of the superoxide anion adduct (DPhPMPO-OOH adduct shown by the separation between the bars in the spectra shown in (**a**)) was determined (**b**). NADPH oxidase activities in cells were determined as described in the Materials and Methods and expressed relative to vehicle-treated controls (**c**). (**d**–**f**), mice were treated once only with or without (vehicle) PPE (100 μg per mouse) and cells in BALF were collected 24 h later. Cells were incubated with DPhPMPO in the presence of indicated concentrations of mepenzolate (μg ml^{-1}) or 100 μM apocynin for 60 min. The level of superoxide anions was determined as described above (**d**,**e**). Cells were pre-incubated with or without mepenzolate (100 μg ml^{-1}) for 3 h and further incubated with NADPH in the presence or absence of PMA (10 ng ml^{-1}) for 20 min. NADPH oxidase activity was determined as described above (**f**). Values represent the mean ± s.e.m. *$P<0.05$; **$P<0.01$ (Tukey test). Experiments were replicated at least two times.

Table 1 | List of gene sets that were differently expressed at 25 h after administration of mepenzolate.

Gene set	NES*†	*P*-value†	FDR‡
Ribosome	2.866	<0.001	<0.001
T-cell receptor signaling pathway	2.066	<0.001	0.018
Drug metabolism cytochrome P450	2.030	<0.001	0.015
Metabolism of xenobiotics by cytochrome P450	1.947	<0.001	0.023
Proteasome	1.799	0.007	0.073
Protein export	1.750	0.021	0.085
Oxidative phosphorylation	1.635	<0.001	0.160
Fatty acid metabolism	1.627	0.023	0.149
Glutathione metabolism	1.567	0.028	0.195
Parkinson's disease	1.471	0.013	0.239

*NES, normalized enrichment score.
†*P*-value, a permutation test implemented in Gene Set Enrichment Analysis (GSEA).
‡FDR, false discovery rate.

muscarinic antagonists, resulting in bronchodilation[28]. Thus, it is reasonable to speculate that mepenzolate, a subtype-non-specific muscarinic receptor antagonist, has bronchodilatory activity as confirmed here. Other subtype-non-specific muscarinic receptor antagonists such as ipratropium and tiotropium examined here did not exert ameliorative effects against PPE-induced pulmonary disorders. Furthermore, scopolamine (a subtype-non-specific muscarinic receptor antagonist) and pirenzepine (an M_1R-specific antagonist) also had no discernible effects against PPE-induced pulmonary disorders, even though, as for mepenzolate, these drugs are orally administered drugs used to treat gastrointestinal disorders and their clinical doses (100 mg per day per adult) are similar to that of mepenzolate (45 mg per day per adult). We also found that the M_2R-specific antagonist gallamine triethiodide and the M_3R-specific antagonist 1,1-dimethyl-4-diphenylacetoxypiperidinium iodide did not affect the PPE-induced increase in number of total leukocytes or neutrophils in BALF (Supplementary Fig. S7). These results suggest that mepenzolate achieves its ameliorative effect against PPE-induced pulmonary disorders *via* mechanisms that are independent of its muscarinic receptor and bronchodilatory activities. On the other hand, glycopyrronium suppressed PPE-induced airspace enlargement and alterations of lung mechanics. The chemical structure of glycopyrronium is similar